J. Fluid Mech. (1978), *vol.* 84, *part* 1, *pp.* 79–111
Printed in Great Britain

A numerical-solution technique for three-dimensional Stokes flows, with application to the motion of strongly interacting spheres in a plane

By PETER GANATOS, ROBERT PFEFFER AND SHELDON WEINBAUM
The City College of The City University of New York

(Received 21 September 1976 and in revised form 30 May 1977)

This paper describes how the collocation technique previously developed by the authors for treating both unbounded (Gluckman, Pfeffer & Weinbaum 1971; Leichtberg, Weinbaum, Pfeffer & Gluckman 1976) and bounded (Leichtberg, Pfeffer & Weinbaum 1976) multiparticle axisymmetric Stokes flows can be extended to handle a wide variety of non-axisymmetric creeping-motion problems with planar symmetry where the boundaries conform to more than a single orthogonal co-ordinate system. The present paper examines in detail the strong hydrodynamic interaction between two or more closely spaced identical spheres in a plane. The various two-sphere configurations provide a convenient means of carefully testing the accuracy and convergence of the numerical solution technique for three dimensional flow with known exact spherical bipolar solutions.

The important difficulty encountered in applying the collocation technique to multiparticle non-axisymmetric flows is that the selection of boundary points is rather sensitive to the flow orientation. Despite this shortcoming one is able to obtain solutions for the quasi-steady particle velocities and drag for as many as 15 spheres in less than 30 s on an IBM 370/168 computer. The method not only gives accurate global results, but is able to predict the local fluid velocity and to resolve fine features of the flow such as the presence of separated regions of closed streamlines. Time-dependent numerical solutions are also presented for various three-sphere assemblages falling in a vertical plane. These solutions, in which the motion of each sphere is traced for several hundred diameters, are found to be in very good agreement with experimental measurements. The concluding section of the paper describes how the present collocation procedure can be extended to a number of important unsolved three-dimensional problems in Stokes flow with planar symmetry such as the arbitrary off-axis motion of a sphere in a circular cylinder or between parallel walls, or the motion of a neutrally buoyant particle at the entrance to a slit or pore.

1. Introduction

The purpose of the present paper is to develop the rudiments of an efficient numerical solution technique which could be used to treat a wide variety of previously unsolved non-axisymmetric creeping-motion problems with planar symmetry where the boundaries conform to more than a single orthogonal co-ordinate surface. Some salient examples of such motion include the settling of three or more closely spaced spheres in

a plane, the arbitrary off-axis motion of a sphere in a circular cylinder or a channel, the tumbling of a spheroid near a planar boundary, and the entrance motion of a sphere into a circular pore or a two-dimensional slit. Problems with strong hydrodynamic interaction of this nature are not easily tractable by perturbation or method-of-reflexion techniques. The two principal difficulties are the slow algebraic decay of three-dimensional disturbances in Stokes flow and the slow convergence properties of an iterative solution scheme when the leading term differs greatly from the desired converged solution.

In the past few years several important advances have been made in the numerical treatment of some of the more complicated boundary-value problems in Stokes flow. These advances, with the exception of the numerical investigation of Youngren & Acrivos (1975), have been limited to axisymmetric motions. For these motions the simplification afforded by the Stokes stream function allows one to reduce the governing equation for quasi-steady creeping motion to the compact form $D^2D^2\psi = 0$. The first highly accurate numerical solutions of this equation by collocation techniques were presented by Skalak and co-workers for several different flow problems involving an infinite array of identical particles periodically spaced along the axis of a circular cylinder. Approximate collocation procedures had previously been used by O'Brien (1968) and others with varying degrees of success. Wang & Skalak (1969), Chen & Skalak (1970) and Hyman & Skalak (1972) considered periodic coaxial arrays of spheres, spheroids and spheroidal bubbles respectively. This problem was then further generalized to an infinite periodic array of arbitrarily shaped axisymmetric particles using a finite-element approach in Skalak, Chen & Chien (1972). These studies of bounded periodic cells were largely motivated by an attempt to model the flow of red cells in the microcirculation.

The interests of the present authors have focused more on time-dependent multiparticle Stokes' flow interactions. For flow problems of this nature one needs rapidly to compute the flow field and quasi-steady drag resulting from the instantaneous interaction of a finite array of particles with arbitrary spacing and velocity. To this end the authors have developed in several previous papers a boundary or collocation technique which can be applied to both unbounded and bounded axisymmetric flows past arbitrary coaxial configurations of spheres and spheroids. The technique developed is capable of calculating in a few seconds on an IBM 370/168 computer both the instantaneous drag and the instantaneous velocity field for as many as 100 spheres or 15 spheroids in unbounded flow with an accuracy for the drag on each particle of better than 0·1 % (Gluckman *et al.* 1971). For unbounded axisymmetric flow the selection of boundary points is not critical except for very close spacings (less than 0·1 diameters), where a judicious selection of boundary points near the axis (Leichtberg, Weinbaum, Pfeffer & Gluckman 1976) allows extension of the range of validity to less than 10^{-4} diameters with little change in computational time. The method has recently been extended to an arbitrary coaxial array of spheres in a circular cylinder (Leichtberg, Pfeffer & Weinbaum 1976), but the computational times required are about two orders of magnitude larger than for the equivalent unbounded case.

The great rapidity with which the unbounded quasi-steady solutions can be obtained for small sphere clusters (in about 10^{-2} s for three or four spheres on an IBM 370/168) has made it possible to follow the time-dependent interaction of small coaxial groupings of spheres over hundreds of diameters and carefully document the importance of

both the unsteady virtual-mass force and the Basset force (the force which arises from the time history of the $\partial \mathbf{V}/\partial t$ term in the unsteady Stokes-flow equation) in multiparticle flows when the flow configuration is slowly changing owing to particle interactions (Leichtberg, Weinbaum, Pfeffer & Gluckman 1976).

In another, biologically related paper (Leichtberg, Weinbaum & Pfeffer 1976) the authors model the time-dependent multiparticle hydrodynamic interaction leading to the aggregation of identical red cells (rouleaux) in the microcapillaries by following the time-dependent motion of identical spheres along the axis of an unbounded Poiseuille profile.

The particles in all the foregoing axisymmetric investigations have been represented by a truncated series of internal singularities derived from the separable solutions of $D^2D^2\psi = 0$ in the appropriate co-ordinate system. For an arbitrary boundary shape one must resort to either finite-difference or finite-element solutions of the entire flow field or represent the body by a surface distribution of singularities (Gluckman, Weinbaum & Pfeffer 1972; Youngren & Acrivos 1975). In Gluckman *et al.* (1972) the flow past an arbitrary convex body of revolution is treated using a surface distribution of spheroidal singularities of vanishing aspect ratio. The integral equation describing this surface distribution is solved using a collocation procedure equivalent to that previously developed by the authors for axisymmetric multiparticle flow. Youngren & Acrivos (1975) present the first numerical solution procedure capable of handling the creeping flow past an arbitrary isolated three-dimensional body. The flow disturbance produced by the body is formulated as an integral equation whose kernel is the fundamental Stokeslet solution of the creeping-motion equation in three dimensions. This integral equation is solved numerically by dividing the body surface into a finite number of discrete elements in each of which the Stokeslet strength is assumed constant.

The integral-equation technique of Youngren & Acrivos is a very promising new approach for treating irregular boundary problems in creeping motion such as the flow past deforming flexible particles and bubbles. However, for a wide variety of three-dimensional problems in Stokes flow when each boundary conforms to a different orthogonal co-ordinate surface (such as the various examples cited at the beginning of this introduction), it is computationally more efficient to develop collocation techniques similar to those just summarized for axisymmetric flow. This approach would take advantage of the various known separable solutions of the Stokes equations in three dimensions. The basic departure from axisymmetric flow is that the fundamental solutions are given in terms of the components of the velocity field rather than a Stokes stream function. These fundamental solutions for the velocity field are known for rectangular, cylindrical, spherical (Lamb 1945, p. 594) and spheroidal (Jeffery 1922) co-ordinates. In theory, the present method could be applied to bounded flow problems where the particles do not conform to natural co-ordinate surfaces using the extensions developed in Gluckman *et al.* (1972) for axisymmetric flow. However, in practice computation times would be prohibitively long. The more general integral-equation approach of Youngren & Acrivos would be more practical for these problems.

A cardinal rule for the successful application of the collocation technique is that the velocity disturbance produced by each co-ordinate boundary may be represented by an ordered sequence of fundamental solutions appropriate to the constant orthogonal

co-ordinate surface to be described. As demonstrated in the appendix to Gluckman *et al.* (1972), the numerical solution can oscillate unstably as the number of collocation points is increased if an inappropriate set of fundamental solutions is used.

Many previously unsolved three-dimensional flows can be constructed from a superposition of two or more truncated series of fundamental solutions from the four basic co-ordinate systems mentioned in the last paragraph. Only minor modifications of the basic collocation scheme described herein for multiple spheres are required to treat spheroids instead of spheres or to combine spheres of different sizes; see Gluckman *et al.* (1971), where the equivalent problem is treated for axisymmetric flow. Also, as outlined in the concluding section, the important extension from unbounded to bounded flow, while very laborious because of the co-ordinate transformations involved, is straightforward and follows the same general procedure as has already been performed for axisymmetric flow in Leichtberg, Pfeffer & Weinbaum (1976). The exact no-slip boundary conditions are imposed along the boundaries of the system, whether they be that of a plane, channel or circular cylinder, and the problem is reduced to a collocation procedure applied along the boundaries of each particle. For all the above reasons the logical starting point in the development of a collocation technique for three-dimensional flows is the basic interaction between two or more spheres using Lamb's (1945, p. 594) spherical-harmonic series solutions for each sphere. The two-sphere problem is itself of special importance since it will enable us carefully to examine the accuracy and convergence of the three-dimensional collocation technique by comparison with exact spherical bipolar solutions. This comparison is essential since the difficulty in constructing a collocation technique is not its formulation, which is conceptually simple, but the detailed development of the truncation. While there is no assurance that the treatment of boundary points for two spheres can be carried over to three or more spheres, the detailed comparison with experiment (described in §5) and with previous multisphere axisymmetric solutions provides some confidence that this is indeed the case.

Although the primary motivation for this paper is to lay the foundations for a more general numerical treatment of bounded three-dimensional creeping motions, it is worth mentioning that the current study is, to the authors' knowledge, the first strong-interaction theory for the non-axisymmetric motion of three or more spheres. Many of the flow configurations described in §5 have been observed experimentally by Jayaweera, Mason & Slack (1964) and studied theoretically in a qualitative manner using a weak-interaction first-order reflexion theory by Hocking (1964).

Section 2 contains the mathematical formulation of the basic collocation technique for an arbitrary planar configuration of N spheres. In §3 solutions obtained by this method are compared with the exact solutions of Stimson & Jeffery (1926) for two equal spheres moving parallel to their line of centres and Goldman, Cox & Brenner (1966) for two equal spheres in an arbitrary orientation. Solutions for instantaneous configurations of three or more spheres are presented in §4. In §5 quasi-steady time-dependent solutions are presented for the trajectories of three spheres settling in a vertical plane starting from various initial configurations. Finally, in §6 the extension of the collocation technique to bounded three-dimensional flows with planar symmetry is discussed.

2. Formulation for multiple spheres

In accord with the comments in the introduction we consider the slow motion of a finite number of equal spheres in an arbitrary asymmetric planar configuration. Consider the steady-state creeping-motion governing equations

$$\mu\nabla^2\mathbf{V} = \nabla p, \quad \nabla.\mathbf{V} = 0, \tag{2.1a, b}$$

where the symbols have their usual meaning. The fundamental solution of (2.1) which is capable of describing an arbitrary disturbance on the surface of a sphere of radius a is given in Happel & Brenner (1973, p. 65):

$$\mathbf{V} = \sum_{n=1}^{\infty}\left[\nabla\times(\mathbf{r}\chi_{-(n+1)}) + \nabla\Phi_{-(n+1)} - \frac{(n-2)}{\mu 2n(2n-1)} r^2\nabla P_{-(n+1)} + \frac{(n+1)}{\mu n(2n-1)}\mathbf{r}P_{-(n+1)}\right]. \tag{2.2}$$

Here $\chi_{-(n+1)}$, $\Phi_{-(n+1)}$ and $P_{-(n+1)}$ are solid spherical harmonic functions of order $-(n+1)$ and $\mathbf{r}$ is the radial position vector, whose origin is at the centre of the sphere.

For the simplest case of N spheres moving slowly in an unbounded quiescent fluid, the linear superposition of N solutions for an individual particle yields

$$\mathbf{V} = \sum_{j=1}^{N}\sum_{n=1}^{\infty}\left[\nabla\times(\mathbf{r}_j\chi_{-(n+1)}(r_j,\theta_j,\phi_j) + \nabla\Phi_{-(n+1)}(r_j,\theta_j,\phi_j) - \frac{(n-2)}{\mu 2n(2n-1)} r_j^2\nabla P_{-(n+1)}(r_j,\theta_j,\phi_j) + \frac{(n+1)}{\mu n(2n-1)}\mathbf{r}_j P_{-(n+1)}(r_j,\theta_j,\phi_j)\right], \tag{2.3}$$

where r_j, θ_j and ϕ_j are spherical co-ordinates measured from the centre of the jth sphere. Equation (2.3) will be generalized in §6 to include an incident stream and confining walls.

In general, the three solid spherical harmonic functions in (2.3) have the following form:

$$\begin{Bmatrix}\chi_{-(n+1)}\\ \Phi_{-(n+1)}\\ P_{-(n+1)}\end{Bmatrix} = \sum_{m=0}^{n} P_n^m(\zeta_j)\frac{1}{r_j^{n+1}}\left[\begin{Bmatrix}A_{jmn}\\ C_{jmn}\\ E_{jmn}\end{Bmatrix}\cos m\phi_j + \begin{Bmatrix}B_{jmn}\\ D_{jmn}\\ F_{jmn}\end{Bmatrix}\sin m\phi_j\right], \tag{2.4}$$

where P_n^m is the associated Legendre function, $\zeta_j = \cos\theta_j$ and A_{jmn}, ..., F_{jmn} are unknown constants which are determined from boundary conditions.

If we now restrict the N spheres to fall freely under gravity in the vertical plane $y = 0$ as shown in figure 1, the symmetry of the flow about this plane requires that

$$A_{jmn} = D_{jmn} = F_{jmn} = 0. \tag{2.5}$$

To perform the operations indicated by (2.3) we express the r_j, ζ_j and ϕ_j in terms of a single rectangular co-ordinate system as shown in figure 1, i.e.

$$r_j^2 = (x-b_j)^2 + y^2 + (z-d_j)^2, \tag{2.6a}$$

$$\zeta_j = \frac{z-d_j}{r_j} = \frac{z-d_j}{[(x-b_j)^2+y^2+(z-d_j)^2]^{\frac{1}{2}}}, \tag{2.6b}$$

$$\tan\phi_j = y/(x-b_j), \tag{2.6c}$$

where b_j and d_j are the x and z co-ordinates of the jth sphere's centre respectively.

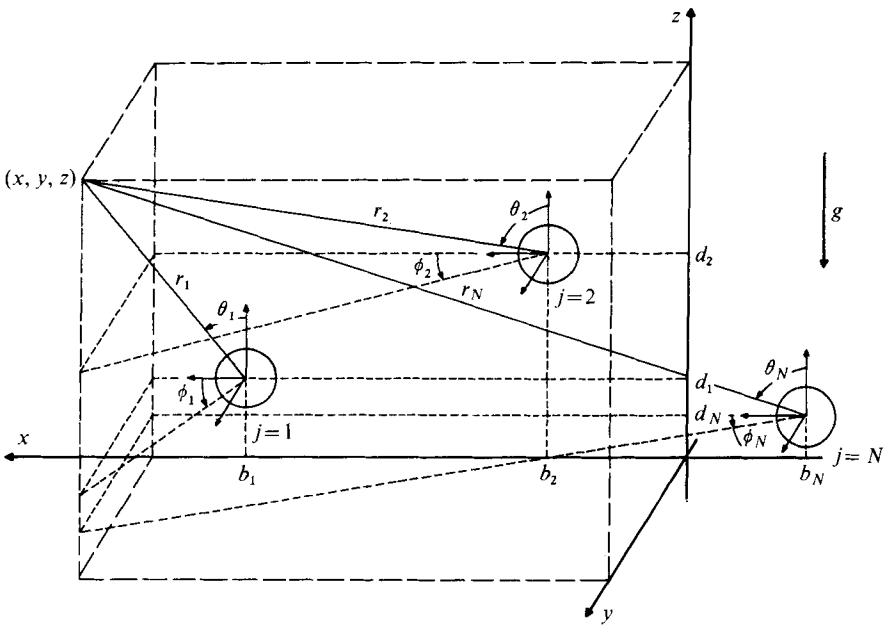

FIGURE 1. Geometry for system of spheres falling freely in a vertical plane.

If u, v and w denote the components of the fluid velocity $\mathbf{V}$ in the x, y and z directions respectively, the no-slip boundary conditions which must be satisfied on the surface of each sphere are

$$u|_{r_j=a} = U_j + a\omega_j \cos\theta_j, \tag{2.7a}$$

$$v|_{r_j=a} = 0, \tag{2.7b}$$

$$w|_{r_j=a} = W_j - a\omega_j \sin\theta_j \cos\phi_j, \tag{2.7c}$$

where a is the radius of each sphere and U_j, W_j and ω_j represent the unknown horizontal, vertical and angular velocity of the jth sphere respectively.

The hydrodynamic force and torque exerted on the jth sphere are given by Happel & Brenner (1973, p. 67) as

$$\mathbf{F}_j = -4\pi\nabla(r_j^3 P_{-2}) \tag{2.8a}$$

and

$$\mathbf{T}_j = -8\pi\mu\nabla(r_j^3\chi_{-2}). \tag{2.8b}$$

Substituting (2.4)–(2.6) into (2.8) gives the simple result

$$\mathbf{F}_j = -4\pi[E_{j11}\,\hat{\mathbf{i}} + E_{j01}\,\hat{\mathbf{k}}] \tag{2.9a}$$

and

$$\mathbf{T}_j = -8\pi\mu B_{j11}\hat{\boldsymbol{j}}. \tag{2.9b}$$

The balance between buoyancy and Stokes drag requires

$$-4\pi[E_{j11}\,\hat{\mathbf{i}} + E_{j01}\,\hat{\mathbf{k}}] + \tfrac{4}{3}\pi a^3(\rho_s - \rho)\,g\hat{\mathbf{k}} = 0 \tag{2.10a}$$

while the condition of zero torque yields

$$-8\pi\mu B_{j11} = 0. \tag{2.10b}$$

Equations (2.10) allow $3N$ of the unknown constants in (2.4) to be determined, i.e.

$$E_{j11} = 0, \quad E_{j01} = \tfrac{1}{3}a^3(\rho_s - \rho)\,g, \quad B_{j11} = 0 \quad (j = 1, 2, 3, \ldots, N). \tag{2.11}$$

This is exactly equal to the number of unknown velocities introduced by (2.7).

Now, if the three no-slip boundary conditions are satisfied at M points on each of the N spheres and the inner two series in (2.3) are truncated to yield a total of $3M$ terms, then a set of $3 \times N \times M$ simultaneous linear algebraic equations results for the $3 \times N \times M$ unknown constants: B_{jmn} ($m \neq 1$ when $n = 1$), C_{jmn}, E_{jmn} ($m \neq 0, 1$ when $n = 1$), U_j, W_j and ω_j. For each point on the surface of the jth sphere at which the three no-slip boundary conditions are satisfied the following equations are obtained:

$$u|_{r_j=a} = \sum_{j=1}^{N} \underbrace{\sum_{n=1}^{} \sum_{m=0}^{n}}_{M\text{terms}} [B_{jmn}B'_{jmn} + C_{jmn}C'_{jmn} + E_{jmn}E'_{jmn}] = U_j + a\omega_j \cos\theta_j, \tag{2.12a}$$

$$v|_{r_j=a} = \sum_{j=1}^{N} \underbrace{\sum_{n=1}^{} \sum_{m=0}^{n}}_{M\text{terms}} [B_{jmn}B''_{jmn} + C_{jmn}C''_{jmn} + E_{jmn}E''_{jmn}] = 0, \tag{2.12b}$$

$$w|_{r_j=a} = \sum_{j=1}^{N} \underbrace{\sum_{n=1}^{} \sum_{m=0}^{n}}_{M\text{terms}} [B_{jmn}B'''_{jmn} + C_{jmn}C'''_{jmn} + E_{jmn}E'''_{jmn}] = W_j - a\omega_j \sin\theta_j \cos\phi_j. \tag{2.12c}$$

Equations (2.12) form the fundamental matrix equation of the collocation technique for planar multiple-sphere configurations. The primed coefficients of the constants B_{jmn}, C_{jmn} and E_{jmn} depend only on the geometry of the flow configuration and are given by

$$B'_{jmn} = \frac{1}{r_j^{n+1}}\left[-\sin\theta_j \sin\phi_j \frac{dP_n^m(\zeta_j)}{d\zeta_j} \sin m\phi_j + m\frac{\cos\phi_j}{\tan\theta_j} P_n^m(\zeta_j) \cos m\phi_j\right], \tag{2.13a}$$

$$C'_{jmn} = \frac{1}{r_j^{n+2}}\left[-\left((n+1)P_n^m(\zeta_j) + \zeta_j \frac{dP_n^m(\zeta_j)}{d\zeta_j}\right)\sin\theta_j \cos\phi_j \cos m\phi_j + m\frac{\sin\phi_j}{\sin\theta_j} P_n^m(\zeta_j) \sin m\phi_j\right], \tag{2.13b}$$

$$E'_{jmn} = \frac{1}{2\mu(2n-1)\,r_j^n}\left[\left((n+1)P_n^m(\zeta_j) + \frac{n-2}{n}\zeta_j \frac{dP_n^m(\zeta_j)}{d\zeta_j}\right) \times \sin\theta_j \cos\phi_j \cos m\phi_j - \frac{m(n-2)}{n}\frac{\sin\phi_j}{\sin\theta_j} P_n^m(\zeta_j) \sin m\phi_j\right], \tag{2.13c}$$

$$B''_{jmn} = \frac{1}{r_j^{n+1}}\left[\sin\theta_j \cos\phi_j \frac{dP_n^m(\zeta_j)}{d\zeta_j} \sin m\phi_j + m\frac{\sin\phi_j}{\tan\theta_j} P_n^m(\zeta_j) \cos m\phi_j\right], \tag{2.13d}$$

$$C''_{jmn} = \frac{1}{r_j^{n+2}}\left[-\left((n+1)P_n^m(\zeta_j) + \zeta_j \frac{dP_n^m(\zeta_j)}{d\zeta_j}\right)\sin\theta_j \sin\phi_j \cos m\phi_j - m\frac{\cos\phi_j}{\sin\theta_j} P_n^m(\zeta_j) \sin m\phi_j\right], \tag{2.13e}$$

$$E''_{jmn} = \frac{1}{2\mu(2n-1)\,r_j^n}\left[\left((n+1)P_n^m(\zeta_j) + \frac{n-2}{n}\zeta_j \frac{dP_n^m(\zeta_j)}{d\zeta_j}\right) \times \sin\theta_j \sin\phi_j \cos m\phi_j + \frac{m(n-2)}{n}\frac{\cos\phi_j}{\sin\theta_j} P_n^m(\zeta_j) \sin m\phi_j\right], \tag{2.13f}$$

$$B'''_{jmn} = -\frac{m}{r_j^{n+1}} P_n^m(\zeta_j) \cos m\phi_j, \tag{2.13g}$$

$$C'''_{jmn} = \frac{1}{r_j^{n+2}} (m-n-1) P_{n+1}^m(\zeta_j) \cos m\phi_j, \tag{2.13h}$$

$$E'''_{jmn} = \frac{1}{2\mu n(2n-1) r_j^n} [2(n+1)\zeta_j P_n^m(\zeta_j) + (n-2)(n-m+1) P_{n+1}^m(\zeta_j)] \cos m\phi_j \tag{2.13i}$$

and

$$\frac{dP_n^m(\zeta_j)}{d\zeta_j} = \frac{(n+1)\zeta_j P_n^m(\zeta_j) - (n-m+1) P_{n+1}^m(\zeta_j)}{1-\zeta_j^2}. \tag{2.14}$$

The system of linear equations described by (2.12) and (2.13) can be solved by any standard matrix reduction technique. It should be noted that, for $m = 0$,

$$B'_{jmn} = B''_{jmn} = B'''_{jmn} = 0.$$

Thus for $m = 0$ the B_{jmn} terms contribute nothing to the solution and should be replaced by the terms of next higher order in the series in order to conserve an equal number of equations and unknown quantities. Thus the sequence in which the terms in (2.12) are taken for each sphere is C_{j01}, E_{j01}, B_{j11}, C_{j11}, E_{j11}, C_{j02}, E_{j02}, B_{j12}, C_{j12}, E_{j12}, ...

In computing and presenting the results for the multiple-sphere problem, it is convenient to non-dimensionalize the physical quantities involved by using the sphere radius as the basic unit of length and the terminal settling velocity U_t of a single isolated sphere as the characteristic velocity:

$$U_t = 2a^2(\rho_s - \rho) g/9\mu. \tag{2.15}$$

Denoting dimensionless variables with a tilde, the non-dimensional horizontal, vertical and angular velocities are defined as

$$\tilde{U}_j \equiv U_j/U_t, \quad \tilde{W}_j \equiv W_j/U_t, \quad \tilde{\omega}_j \equiv a\omega_j/U_t \tag{2.16}$$

and the dimensionless time as

$$\tilde{t} \equiv U_t t/a. \tag{2.17}$$

The hydrodynamic force exerted on the jth sphere in the presence of all the other spheres can alternatively be expressed as

$$\mathbf{F}_j \equiv -6\pi\mu a[U_j \lambda_{Hj} \hat{\mathbf{i}} + W_j \lambda_{Vj} \hat{\mathbf{k}}], \tag{2.18}$$

where λ_{Hj} and λ_{Vj} are the horizontal and vertical drag correction factors defined by (2.18). Comparing this equation with (2.9a) and using (2.11), (2.15) and (2.16) one finds that

$$\lambda_{Hj} = E_{j11}/1{\cdot}5\mu a U_j = 0 \quad \text{when} \quad U_j \neq 0, \tag{2.19a}$$

$$\lambda_{Vj} = E_{j01}/1{\cdot}5\mu a W_j = 1/\tilde{W}_j. \tag{2.19b}$$

In subsequent sections λ_{Vj} will be denoted simply as λ_j since, from (2.19a), $\lambda_{Hj} = 0$.

3. Two-sphere solutions

In this section the accuracy and convergence of the basic collocation technique described in § 2 will be carefully examined by comparing the present results with the

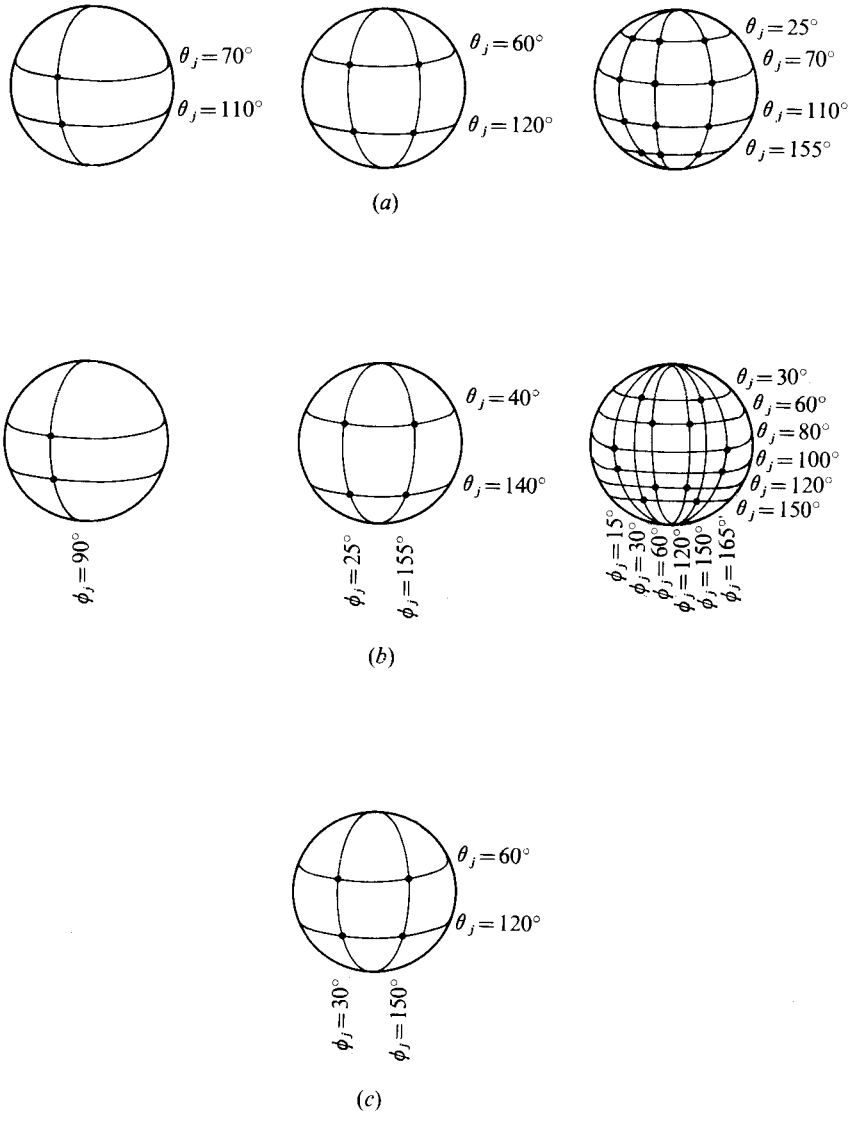

FIGURE 2. Position of points for spheres falling (*a*) parallel to their line of centres, (*b*) perpendicular to their line of centres and (*c*) in an arbitrary orientation.

exact two-sphere solutions of Stimson & Jeffery (1926) and Goldman *et al.* (1966). Also, the sensitivity of the solution to the selection of boundary points will be explored. In essence we wish to study the truncation properties of the matrix equation (2.12).

When specifying the points along the boundary of each sphere where conditions (2.7) are to be exactly satisfied, it is necessary to choose a pattern which is symmetric about both the equatorial plane $\theta_j = \frac{1}{2}\pi$ and the meridional plane $\phi_j = \frac{1}{2}\pi$. Owing to the symmetry about the plane $y = 0$ only the flow in the region $y \geqslant 0$ need be considered. Thus the range for θ_j and ϕ_j is between 0 and π and the points chosen should lie on this hemisphere.

Trials using up to twelve boundary points on each hemisphere were made for two equal spheres falling perpendicular and parallel to their line of centres at various

Spacing	Exact solution	$M = 2$	$M = 4$	$M = 12$
10	0·93036	0·93045	0·93040	0·93036
9	0·92325	0·92336	0·92331	0·92325
8	0·91454	0·91469	0·91461	0·91454
7	0·90360	0·90381	0·90371	0·90360
6	0·88949	0·88978	0·88966	0·88949
5	0·87060	0·87103	0·87088	0·87060
4	0·84412	0·84477	0·84462	0·84412
3	0·80472	0·80559	0·80573	0·80470
2	0·74226	0·74200	0·74458	0·74216
1·8884	0·73325	0·73247	0·73580	0·73314
1·5431	0·70245	0·69854	0·70576	0·70229
1·3374	0·68205	0·67450	0·68580	0·68192
1·1276	0·65963	0·64623	0·66371	0·65963
1·0453	0·65037	0·63391	0·65443	0·65043
1·0050	0·64572	0·62758	0·64973	0·64581
1·0025	0·64543	0·62717	0·64943	0·64552
1	0·64514	0·62678	0·64914	0·64524

TABLE 1. Comparison of the solutions for the drag correction factor λ_j obtained by the collocation technique with the exact solution for two equal spheres falling parallel to their line of centres.

spacings. The sphere spacing d_{12} is defined as the centre-to-centre distance between two equal spheres measured in sphere diameters. The only solutions found to give meaningful results were the $M = 2$, 4 and 12 solutions. Intermediate values of M were unsuccessful owing to one or a combination of the following reasons:

(*a*) Locating points at $\theta_j = 0, \frac{1}{2}\pi, \pi$ or $\phi_j = 0, \frac{1}{2}\pi, \pi$ in many cases produces a singular matrix, so that the symmetry requirements outlined in the previous paragraph cannot be met for odd values of M.

(*b*) The system of equations (2.12) produces an ill-conditioned matrix, i.e. a near-zero determinant, for certain configurations of points.

(*c*) The series (2.12) cannot be arbitrarily truncated at any point. Apparently, when certain terms are retained in the series, they require the presence of other terms for the series to converge uniformly. Thus, in contrast to axisymmetric flow, where boundary points could simply be added in symmetric pairs, the truncation of the matrix equation (2.12) following the particular ordered sequence described in §2, and consequently the number of boundary points taken on each sphere, proceeds in jumps.

Figure 2(*a*) shows the positions of the points used for two equal spheres falling parallel to their line of centres. In this case, the flow is axisymmetric and the solution is independent of the ϕ_j co-ordinate of the points. However, no point should be located at $\phi_j = 0, \frac{1}{2}\pi$ or π since this produces a singular matrix. The results for the drag correction factor at various spacings are compared with the exact values in table 1. Rapid convergence to the exact solution is obtained as the number of points is increased. The maximum error, for the case of touching spheres with only two boundary points on each sphere is only 2·8 %. This is in sharp contrast to the method of reflexions, which gives an error of 26 % at this spacing.

Figure 2(*b*) shows the positions of the points used for two equal spheres falling perpendicular to their line of centres. The two-point solution shown was found to be independent of the θ_j co-ordinate of the points. The results for the vertical drag correc-

Spacing	Exact solution	$M = 2$	$M = 4$	$M = 12$
		Vertical drag correction factor, λ_j		
10	0·96380	0·96384	0·96380	0·96380
9	0·95992	0·95998	0·95992	0·95992
8	0·95511	0·95520	0·95511	0·95511
7	0·94899	0·94911	0·94899	0·94899
6	0·94092	0·94111	0·94092	0·94092
5	0·92981	0·93013	0·92981	0·92980
4	0·91348	0·91410	0·91349	0·91347
3	0·88709	0·88850	0·88711	0·88708
2	0·83680	0·84113	0·83694	0·83677
1·8884	0·82819	0·83324	0·82836	0·82815
1·5431	0·79454	0·80301	0·79490	0·79445
1·3374	0·76751	0·77934	0·76804	0·76739
1·1276	0·73271	0·74887	0·73288	0·73282
1·0453	0·71771	0·73470	0·71648	0·71917
1·0050	0·71255	0·72721	0·70786	0·71523
1·0025	0·71292	0·72673	0·70730	0·71513
1	0·72469	0·72626	0·70676	0·71507
		Angular velocity, $\tilde{\omega}_j$		
10	0·0018750	0·0018633	0·0018759	0·0018750
9	0·0023149	0·0022970	0·0023161	0·0023148
8	0·0029297	0·0029013	0·0029318	0·0029297
7	0·0038265	0·0037781	0·0038300	0·0038265
6	0·0052082	0·0051190	0·0052146	0·0052081
5	0·0074997	0·0073157	0·0075120	0·0074994
4	0·011717	0·011273	0·011744	0·011716
3	0·020824	0·019452	0·020886	0·020818
2	0·046696	0·040249	0·046735	0·046660
1·8884	0·052304	0·044336	0·052288	0·052262
1·5431	0·077498	0·061181	0·076940	0·077470
1·3374	0·10101	0·075186	0·099645	0·10116
1·1276	0·13141	0·093124	0·13120	0·13150
1·0453	0·13664	0·10101	0·14534	0·13119
1·0050	0·11576	0·10495	0·15220	0·11019
1·0025	0·10825	0·10520	0·15262	0·10778
1	0	0·10545	0·15303	0·10531

TABLE 2. Comparison of the solutions obtained by the collocation technique with the exact solution for two equal spheres falling freely side by side at various spacings.

tion factor and the angular velocity at various spacings are compared with the exact values in table 2. Examination of table 2 shows general convergence to the exact solution as the number of boundary points is increased, except for a small deviation for the angular velocity predicted by the four-point solution at very close spacings. This deviation for close spacings is not surprising since, as observed in Leichtberg, Weinbaum, Pfeffer & Gluckman (1976), one needs more boundary points in the vicinity of contact if one is adequately to satisfy the no-slip boundary conditions in the near-collision limit. It is interesting in this regard that the error in the twelve-point solution for both λ_j and $\tilde{\omega}_j$ is only about 0·4 % when the gap between the spheres is 0·0025

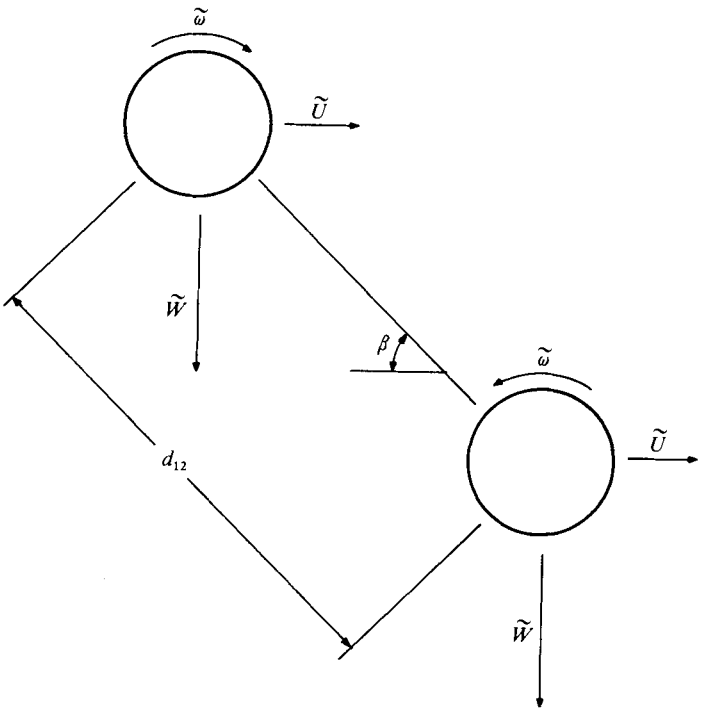

FIGURE 3. Two equal spheres settling in an arbitrary orientation under gravity.

diameters. However, the solution fails to predict zero angular velocity when the spheres touch.

Equally accurate quasi-steady solutions for a straight chain of two or more spheres at any orientation β (see figure 3) may be obtained using formulae (4.1)–(4.3) in the next section, which are based on the highly accurate truncation solutions for $\tilde{\omega}_{\perp j}$, $\lambda_{\parallel j}$ and $\lambda_{\perp j}$. These formulae can obviously not be applied to the arbitrary planar motion of three or more spheres when the sphere configuration is continuously changing owing to particle interactions. For this purpose we examine next the truncation of (2.12) assuming that (4.1)–(4.3) cannot be used.

The solutions shown in tables 1 and 2 for the vertical and horizontal two-sphere configurations exhibit both rapid convergence properties as the number of boundary points is increased from 2 to 4 to 12 and insensitivity to small changes in the location of the boundary points shown in figures 2(*a*) and (*b*). Unfortunately, this behaviour does not extend to the settling of two spheres at an arbitrary orientation β if (4.1)–(4.3) are not used. The difficulty is not the selection of boundary points for a given flow orientation (the selection of boundary points is not a sensitive function of sphere spacing for a given orientation except for small gap widths) but the fact that for each angle β a different set of boundary points should be used. This feature of the collocation technique is its most important shortcoming.

To overcome this difficulty, the angle β may be divided into several different ranges between 0 and $\frac{1}{2}\pi$, and a different set of boundary points used in each range to keep the error in the horizontal drift and angular velocities within acceptable limits. However, satisfactory results may be obtained more conveniently by finding a single optimum

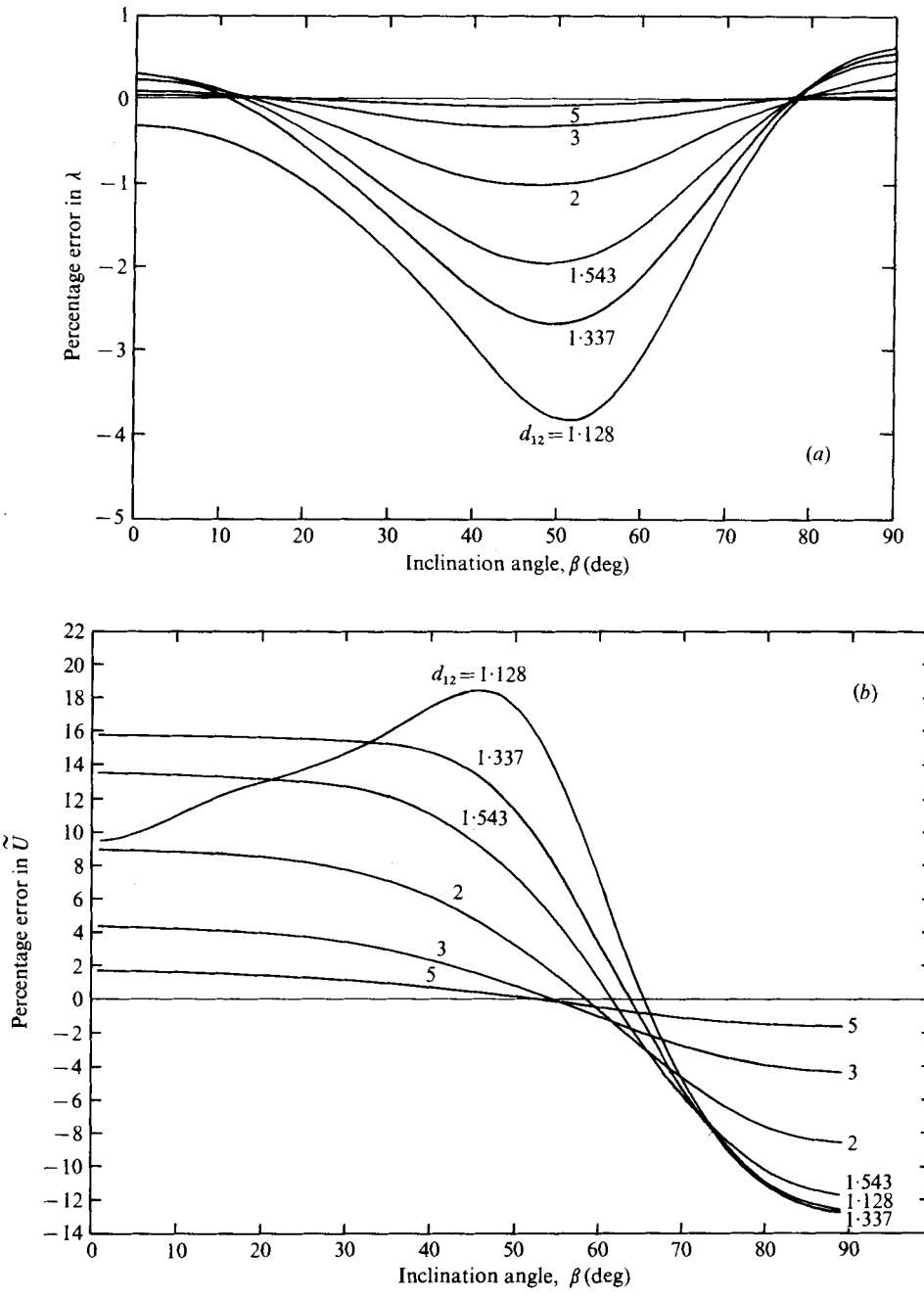

FIGURES 4(*a*, *b*). For legend see next page.

configuration of points which can be used for all orientations. To this end more than 6000 solutions were tested by varying the configuration of points and the orientation angle β. These tests showed that, while a given configuration of points produced good results over a certain range of β, the same set of points could produce substantial errors outside this range. The four-point solution found to give the smallest maximum

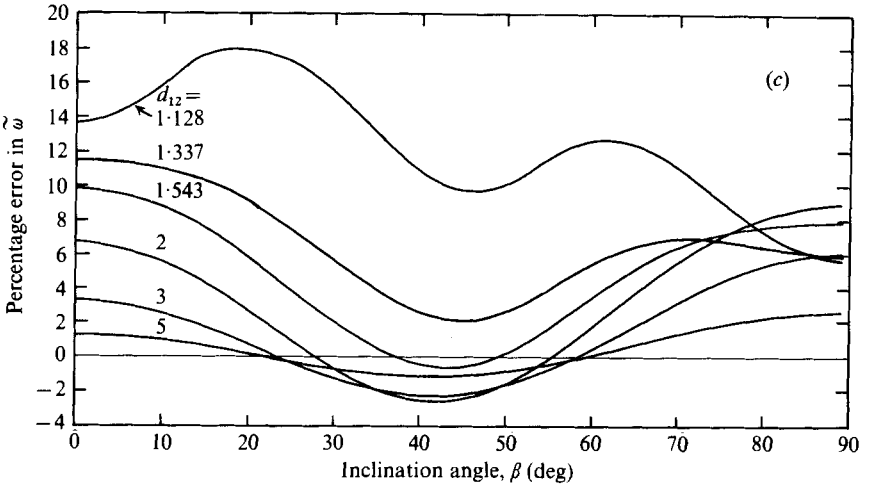

FIGURE 4. Percentage error in (*a*) vertical drag correction factor, (*b*) horizontal drift velocity and (*c*) angular velocity of two equal spheres as a function of orientation at various spacings.

percentage error at any orientation is shown in figure 2 (*c*). The percentage error in the drag, angular velocity and horizontal drift velocity for this positioning of the points is presented as a function of orientation for various spacings d_{12} in figure 4. The maximum error in the vertical drag correction factor occurs in the central range of the orientation angle for all spacings. For spacings of about 1·3 or greater, the maximum error in the horizontal drift velocity and angular velocity occurs when the line of centres is nearly horizontal or vertical. At closer spacings the maximum error in angular velocity and horizontal drift velocity occurs at orientations of roughly 20° and 45° respectively. Even though the percentage errors in the drift and angular velocities seem large for close spacings, it should be kept in mind that the magnitude of these quantities is small and, therefore, their actual deviation is small. The maximum values for the drift and angular velocities at any spacing or orientation are less than 6 and 10 % respectively of the vertical velocity component (Goldman *et al.* 1966). Nevertheless concern about the cumulative effect of small errors for long-time interactions was one of the reasons for performing the experiments presented in § 5.

The four-point solutions shown in figure 4 can be substantially improved over most of the range of β by going to twelve-point solutions. This increases the number of matrix equations to be solved for each sphere from 12 to 36. Thus for time-dependent multisphere interactions involving a thousand or more quasi-steady solutions this improvement is not practical and, as seen at the end of § 5, comparison with experiment shows that such improvement is unwarranted. However, for the single, bounded, non-axisymmetric sphere calculations described in § 6 such improvement would certainly be desired.

A natural question to ask at this point is how accurately the collocation technique can predict the local fluid velocity. Tables 3 shows values of the local fluid velocity $\tilde{W}_f$ relative to the sphere settling velocity $\tilde{W}$ for two spheres settling axisymmetrically at a centre-to-centre spacing of three diameters. This configuration was chosen since the exact local velocity field can easily be computed from the Stimson & Jeffery solution. The $M = 4$ and 12 collocation solutions correspond to those shown in figure

(*a*) *On midplane* ($\tilde{z} = 0$)

Radial distance $\tilde{R}$ (radii)	$\tilde{W}_f - \tilde{W}$ (exact solution)	$\tilde{W}_f - \tilde{W}$ ($M = 4$)	$\tilde{W}_f - \tilde{W}$ ($M = 12$)
0	0·30190	0·29854	0·30195
0·1	0·30281	0·29946	0·30286
0·2	0·30553	0·30222	0·30558
0·3	0·31002	0·30677	0·31007
0·4	0·31624	0·31306	0·31628
0·5	0·32409	0·32100	0·32414
0·6	0·33350	0·33051	0·33354
0·7	0·34434	0·34147	0·34439
0·8	0·35650	0·35375	0·35655
0·9	0·36985	0·36723	0·36989
1·0	0·38425	0·38175	0·38429
1·5	0·46712	0·46519	0·46717
2·0	0·55677	0·55519	0·55681
3·0	0·71744	0·71604	0·71747
4·0	0·83512	0·83368	0·83516
5·0	0·91648	0·91498	0·91651
6·0	0·97328	0·97175	0·97331
7·0	1·01418	1·01264	1·01422
8·0	1·04466	1·04310	1·04469
9·0	1·06809	1·06858	1·06813
10·0	1·08661	1·08505	1·08664

(*b*) *Along axis* ($\tilde{R} = 0$)

Axial distance $\tilde{Z}$ (radii)	$\tilde{W}_f - \tilde{W}$ (exact solution)	$\tilde{W}_f - \tilde{W}$ ($M = 4$)	$\tilde{W}_f - \tilde{W}$ ($M = 12$)
0	0·30190	0·29854	0·30195
0·1	0·30110	0·29773	0·30115
0·2	0·29871	0·29530	0·29876
0·3	0·29470	0·29123	0·29475
0·4	0·28906	0·28549	0·28910
0·5	0·28173	9·27804	0·28178
0·6	0·27269	0·26884	0·27273
0·7	0·26186	0·25781	0·26190
0·8	0·24920	0·24490	0·24924
0·9	0·23464	0·23004	0·23468
1·0	0·21813	0·21315	0·21815
1·1	0·19960	0·19418	0·19962
1·2	0·17906	0·17309	0·17907
1·3	0·15653	0·14991	0·15653
1·4	0·13216	0·12474	0·13213
1·5	0·10624	0·09788	0·10618
1·6	0·07937	0·06990	0·07926
1·7	0·05261	0·04190	0·05244
1·8	0·02785	0·01587	0·02760
1·9	0·00839	−0·00455	0·00806
2·0	0	−0·01269	−0·00038
4·0	0	−0·01614	−0·00032
4·1	0·01359	−0·00105	0·01333
4·2	0·04443	0·03147	0·04424
4·3	0·08317	0·07178	0·08303

Axial distance $\tilde{Z}$ (radii)	$\tilde{W}_f - \tilde{W}$ (exact solution)	$\tilde{W}_f - \tilde{W}$ ($M = 4$)	$\tilde{W}_f - \tilde{W}$ ($M = 12$)
4·4	0·12486	0·11485	0·12477
4·5	0·16689	0·15805	0·16683
4·6	0·20786	0·20001	0·20783
4·7	0·24707	0·24005	0·24706
4·8	0·28422	0·27790	0·28422
4·9	0·31920	0·31347	0·31922
5·0	0·35204	0·34680	0·35206
6·0	0·58720	0·58436	0·58724
7·0	0·72150	0·71934	0·72154
8·0	0·80790	0·80601	0·80794
9·0	0·86842	0·86666	0·86846
10·0	0·91338	0·91169	0·91342

TABLE 3. Comparison between exact Stimson & Jeffery solution and collocation solutions for the local fluid velocity relative to the sphere settling velocity at a spacing of 3 diameters.

(*a*) *On midplane* ($\tilde{z} = 0$)

Radial distance $\tilde{R}$ (radii)	$\tilde{W}_f - \tilde{W}$ (exact solution)	$\tilde{W}_f - \tilde{W}$ (boundary points placed as in figure 2*a*)	$\tilde{W}_f - \tilde{W}$ (boundary points placed near point of interest)
0	0·01255	0·01203	0·01288
0·1	0·01456	0·01410	0·01486
0·2	0·02066	0·02034	0·02085
0·3	0·03093	0·03082	0·03093
0·4	0·04549	0·04561	0·04521
0·5	0·06437	0·06471	0·06375
0·6	0·08751	0·08802	0·08647
0·7	0·11468	0·11532	0·11318
0·8	0·14550	0·14620	0·14352
0·9	0·17945	0·18016	0·17699
1·0	0·21592	0·21659	0·21302
1·5	0·41376	0·41415	0·40950
2·0	0·59564	0·59589	0·59112
3·0	0·84764	0·84788	0·84333
4·0	0·99070	0·99097	0·98653
5·0	1·07697	1·07725	1·07284
6·0	1·13339	1·13367	1·12928
7·0	1·17286	1·17314	1·16875
8·0	1·20194	1·20222	1·19784
9·0	1·22425	1·22452	1·22014
10·0	1·24189	1·24217	1·23778

(*b*) *Along axis* ($\tilde{R} = 0$)

Axial distance $\tilde{z}$ (radii)	$\tilde{W}_f - \tilde{W}$ (exact solution)	$\tilde{W}_f - \tilde{W}$ (boundary points placed as in figure 2*a*)	$\tilde{W}_f - \tilde{W}$ (boundary points placed near point of interest)
0	0·01255	0·01203	0·01288
0·1	0·01181	0·01124	0·01216
0·2	0·00974	0·00898	0·01014
0·3	0·00673	0·00563	0·00717
0·4	0·00345	0·00184	0·00391
0·5	0·000818	−0·00148	0·00121
0·6	−0·000260	−0·00336	−0·000069
0·62	−0·000262	−0·00351	−0·000123
0·64	−0·000211	−0·00358	−0·000122
0·66	−0·000127	−0·00359	−0·000083
0·67	−0·000082	−0·00357	−0·000057
0·68	−0·000041	−0·00356	−0·000032
0·69	−0·000012	−0·00353	−0·000012
0·7	0	−0·00350	0·00000
2·7	0	−0·00272	0·00000
2·71	0·000188	−0·00251	0·000187
2·72	0·000736	−0·00194	0·000736
2·73	0·00162	−0·00102	0·00162
2·74	0·00281	0·00022	0·00282
2·76	0·00605	0·00355	0·00606
2·78	0·01029	0·00790	0·01030
2·8	0·01541	0·01313	0·01541
2·9	0·05035	0·04866	0·05024
3·0	0·09420	0·09302	0·09388
4·0	0·49626	0·49650	0·49359
5·0	0·71865	0·71895	0·71515
6·0	0·85104	0·85134	0·84724
7·0	0·93882	0·93911	0·93489
8·0	1·00150	1·00179	0·99751
9·0	1·04864	1·04892	1·04461
10·0	1·08545	1·08573	1·08140

TABLE 4. Comparison between exact Stimson & Jeffery solution and twelve-point collocation solutions for the local fluid velocity relative to the sphere settling velocity at a spacing of 1·7 diameters.

2(*a*). Examination of table 3 shows that the relative velocities predicted by the collocation solutions are consistently accurate to within about 1 % for $M = 4$ and 0·01 % for $M = 12$ except immediately adjacent to the spheres. The accuracy of the $M = 12$ solution near the sphere axis is very good in light of the fact that there are no boundary points in that vicinity.

Another point of interest is to determine whether the collocation technique is capable of predicting fine features of the flow such as the presence of separated regions of closed streamlines. Davis *et al.* (1976) have used the Stimson & Jeffery solution to show that, for steady, axisymmetric, uniform flow past two equal spheres, separation of the flow from the spheres occurs for centre-to-centre spacings of less than 1·79 diameters. As the spacing is further decreased, the two separated flow regions adjacent to each

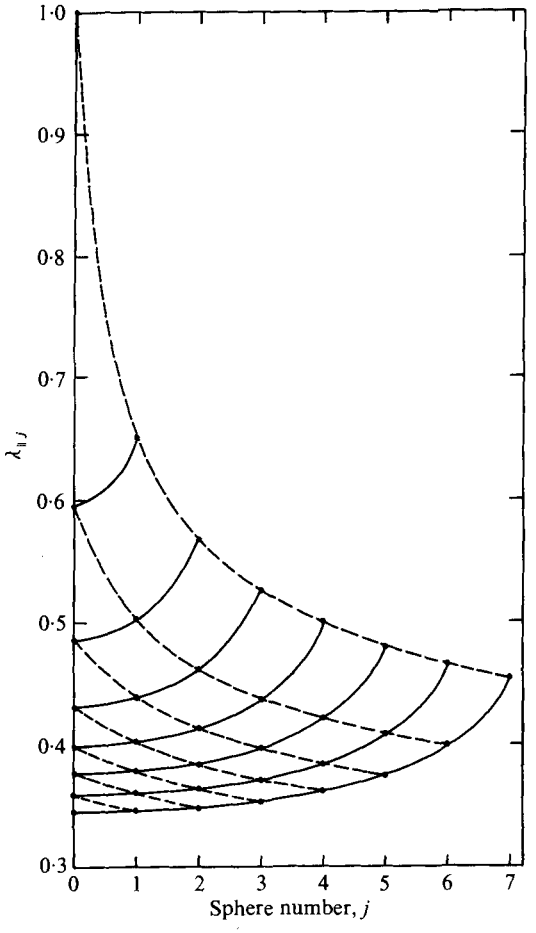

FIGURE 5. Drag correction factor for vertical sphere chains at a spacing $d_{12} = 2$.

sphere coalesce and the region between the two spheres rotates in one or more ring vortices. To see whether the collocation technique can predict this behaviour, values of the relative local fluid velocity were obtained for two spheres settling under gravity at a spacing of 1·7 diameters for the plane midway between the two spheres ($\bar{Z} = 0$) and along the axis (tables 4 (*a*, *b*) respectively). Results are shown for two sets of twelve-point collocations: one as in figure 2 (*a*) and one in which two sets of boundary points were placed near the axis, i.e. at $\theta_j = 1°$ and 179° for three arbitrary values of ϕ_j with the remaining six points placed at $\theta_j = 45°$ and 135° in a scheme similar to that used by Leichtberg, Weinbaum, Pfeffer & Gluckman (1976) to improve the accuracy of the solution in the near-collision limit. Table 4 (*a*) shows that both collocation schemes are in good agreement with the exact solution with a maximum local error of about 1 %. Table 4 (*b*) shows that both collocation schemes predict the presence of the separated flow region in accord with the exact solution. However, the extremely small relative velocities adjacent to the sphere are obscured by the relatively larger slip velocity incurred by using the collocation in figure 2 (*a*). A substantial improvement is observed as the slip velocity is eliminated in this vicinity by placing boundary points near the

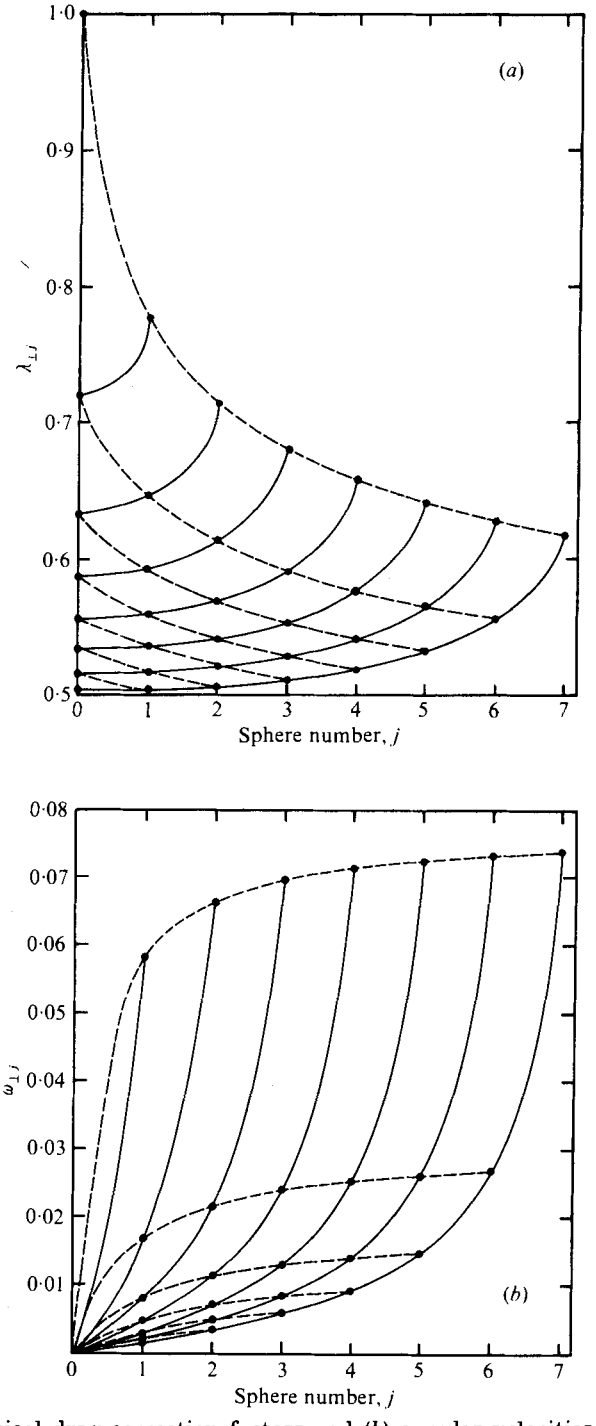

FIGURE 6. (*a*) Vertical drag correction factors and (*b*) angular velocities for horizontal sphere chains at a spacing $d_{12} = 2$.

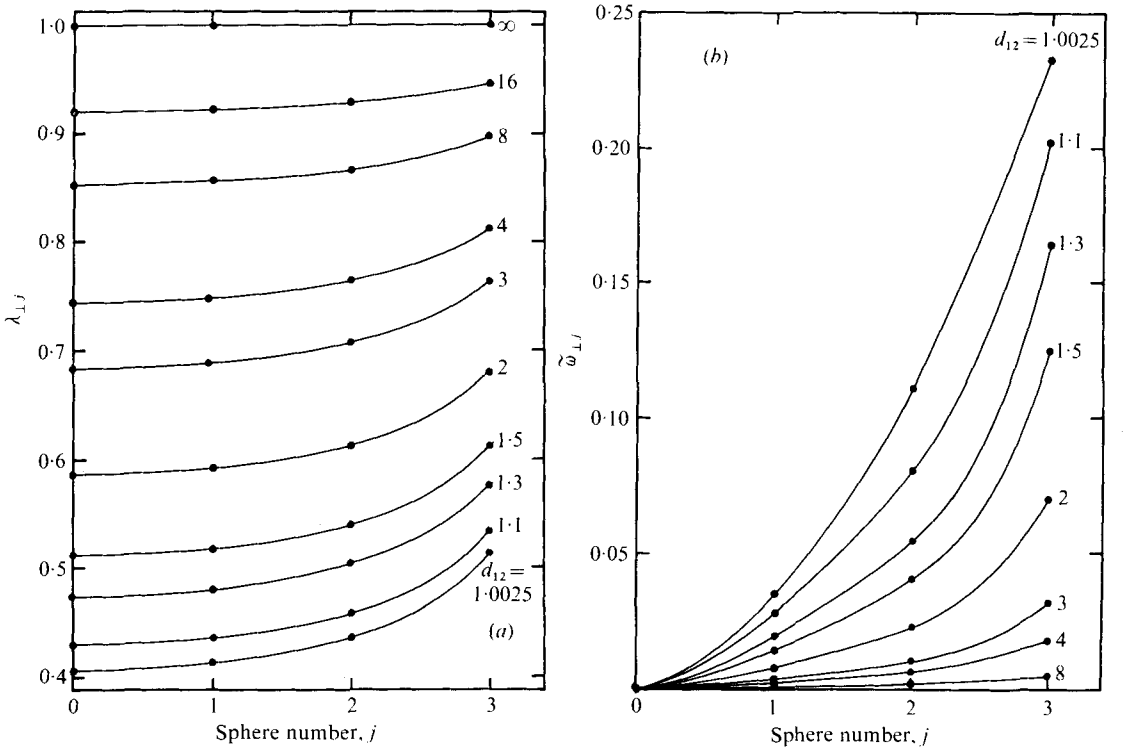

FIGURE 7. (*a*) Vertical drag correction factors and (*b*) angular velocities for a seven-sphere horizontal chain at different sphere spacings.

axis $\tilde{R} = 0$. This modification also produces a considerable improvement in the solution in the vicinity of the other side of the sphere (i.e. for $\tilde{Z} > 2{\cdot}7$). The 12-point collocations also exhibited the various vortex patterns described by Davis *et al.* (1976) at closer spacings.

4. Multiple-sphere configurations

The solutions for the vertical and horizontal two-sphere configurations shown in figures 2 (*a*), (*b*) are readily extended to vertical and horizontal arrays of any number of equally spaced spheres, the only limitation being the size of the matrix (2.12) that the computer can handle. Although these flow configurations are transitory, they do shed important light on the order of magnitude of particle interactions in larger chains, particle shielding effects and the effect of relative spacing and orientation. The results are also the first presented for the angular velocity of three or more closely spaced spheres.

Figure 5 shows the drag correction factor $\lambda_{\parallel j}$ for straight chains containing 3, 5, 7, 9, 11, 13 and 15 equally spaced spheres falling parallel to their line of centres at a spacing of 2 diameters. The central sphere is denoted by $j = 0$. Results are shown for only half of the chains since values for the other half are symmetric about $j = 0$. Solid lines connect solutions through individual spheres in a chain, which are represented by

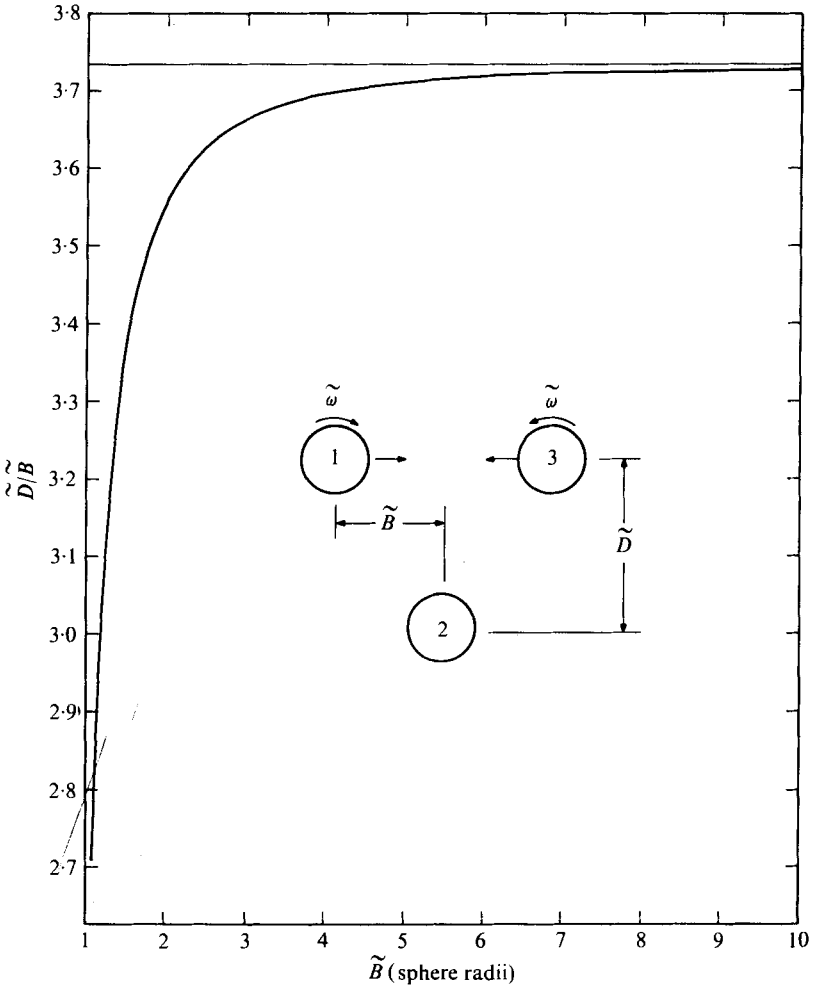

FIGURE 8. Critical spacing for triangular three-sphere configuration.

the points shown. The dashed lines connect spheres of the same number taken from the outermost sphere. The error in $\lambda_{\|j}$ for these four-point solutions is believed to be about 0·3 % on the basis of the results in table 1 and a comparison with the axisymmetric collocation theory of Leichtberg, Weinbaum, Pfeffer & Gluckman (1976).

Figures 6(*a*) and (*b*) show the vertical drag correction factor $\lambda_{\perp j}$ and the angular velocity $\tilde{\omega}_{\perp j}$ for the same chains falling perpendicular to their line of centres. The meaning of the dashed and solid lines is the same as in figure 5. The estimated error for the four-point configuration used is about 0·02 % for the vertical drag correction factors and 0·09 % for the angular velocities; see table 2. The three-, five- and seven-sphere chains were also run using the twelve-point collocation (figure 2*b*) and confirm this estimated accuracy of the four-point solution.

Comparison of figures 5 and 6(*a*) shows that the relative difference between $\lambda_{\|j}$ and $\lambda_{\perp j}$ grows progressively larger as the chain length is increased. One might conjecture that the ratio of $\lambda_\perp$ to $\lambda_\|$ approaches the value 2 in accord with slender-body theory as the chain length becomes infinite. A marked reduction in drag per sphere as the size of

the chain is increased is clearly evident in these figures. (The fifteen-sphere vertical chain falls roughly three times as fast as an isolated sphere.) Examination of figure 6 (*b*) shows how the angular velocity increases as one moves to the outer spheres in a horizontal chain and that for larger chains, as shown by the dashed lines, this variation in angular velocity is very small. Spheres to the left of $j = 0$ rotate clockwise, while spheres to the right rotate counterclockwise. The computation times required to determine the drag and velocity field varied from about 0·75 s for a three-sphere chain to about 30 s for the fifteen-sphere chain using an IBM 370/168 computer.

Figures 7 (*a*) and (*b*) examine the effect of sphere spacing and end effects for a seven-sphere horizontal chain. Related results are presented in Gluckman *et al.* (1971) for vertical chains. These solutions, obtained with the twelve-point configurations shown in figure 2 (*b*), have a maximum probable error for $\lambda_{\perp j}$ of about 0·4 % at $d_{12} = 1{\cdot}0025$. The error in the angular velocities is about 5 % at $d_{12} = 1{\cdot}0025$ and about 0·08 % at $d_{12} = 2$. A chain of seven nearly touching spheres falls more than twice as fast as an isolated sphere, with the central sphere moving about 20 % faster than the outermost one. Figure 7 (*b*) shows that the angular velocity of each sphere in the horizontal chain increases rapidly as the spacing is decreased until a maximum angular velocity is achieved for very small gaps in the lubrication-theory limit. This maximum is observed to occur at a spacing of about 1·05 diameters for two spheres (see table 2) and decreases as more spheres are added to the chain.

The solution for a straight chain of spheres falling in any arbitrary orientation β may be obtained by combining the solutions for a vertical chain and a horizontal chain with the same spacing as was done for the case of two spheres by Goldman *et al.* (1966). If the acute angle between the line of centres and the horizontal is β (see figure 3) the horizontal drift, angular velocity and vertical drag correction factor are given by

$$\tilde{U}_j = \frac{\lambda_{\perp j} - \lambda_{\parallel j}}{2\lambda_{\perp j}\lambda_{\parallel j}} \sin 2\beta, \quad \tilde{\omega}_j = \tilde{\omega}_{\perp j} \cos\beta, \tag{4.1), (4.2}$$

$$\lambda_j = \frac{2\lambda_{\perp j}\lambda_{\parallel j}}{(\lambda_{\perp j} + \lambda_{\parallel j}) - (\lambda_{\perp j} - \lambda_{\parallel j})\cos 2\beta}. \tag{4.3}$$

As mentioned previously, these formulae based on $\omega_{\perp j}$, $\lambda_{\perp j}$ and $\lambda_{\parallel j}$ are considerably more accurate than the more general four-point solutions shown in figures 4 (*a*), (*b*) and (*c*).

In Ganatos (1977) a variety of specialized but intriguing quasi-steady three- and four-sphere configurations are studied. One which is relevant to the time-dependent solutions described in the next section is the three-sphere configuration sketched in figure 8. The question asked is whether there is a critical value of $\tilde{D}/\tilde{B}$ for which all three spheres will fall with the same vertical velocity assuming that sphere 2 is on the centre-line between spheres 1 and 3. The locus of such solutions is shown by the curve in figure 8. The interested reader is referred to the above reference for a more thorough discussion of this and other specialized flow geometries.

5. Time-dependent settling of three spheres in a vertical plane

In general, a cluster of three or more spheres falling asymmetrically in a vertical plane cannot achieve a stable steady-state configuration even after the initial quasi-steady settling velocity is achieved, since the quasi-steady Stokes drag on each sphere

continues to vary because of multiparticle interaction effects that continually change as a function of particle spacing and velocity. As a result, the solutions presented in the previous section are valid for those particular configurations which exist at one instant of time except for certain special cases discussed in Ganatos (1977) where the velocity of all the particles is the same and the configuration does not change.

Unsteady multiparticle creeping motions are complicated by the appearance of Basset, virtual-mass and acceleration forces and by the difficulty of calculating fluid–particle interactions for three or more closely spaced particles. Leichtberg, Weinbaum, Pfeffer & Gluckman (1976) have presented a theoretical and experimental investigation exploring the importance of each of these complicating features by examining in detail the hydrodynamic interaction between three or more spheres falling under gravity along a common axis parallel to their line of centres. The results of this investigation indicated, in general, that the Basset force is the most important unsteady force in gravitational flow at low Reynolds numbers in which the flow configuration is slowly changing owing to fluid–particle interactions. Virtual mass and particle acceleration, on the other hand, were shown to be of negligible importance except for a short-lived initial transient period. Nevertheless, even with the complete omission of the unsteady forces, the qualitative behaviour of the problem was preserved and agreement between theory and experiment was reasonable, especially for runs of short duration in which $Re \leqslant 0{\cdot}1$.

Although a complete theoretical analysis of the settling of clusters of spheres should include all the unsteady forces present, the computations required for including these forces for non-axisymmetric flow are prohibitively time-consuming on present computers. If the unsteady forces are omitted (i.e. at each instant of time it is assumed that the quasi-steady Stokes drag balances the gravitational buoyant forces on each sphere), the numerical integration procedure used to determine the trajectory and rotation of each sphere for a typical run requires that the system of equations given by (2.12) and (2.13) be solved between 1000 and 3000 times for runs of the order of 1000 sphere diameters. To accomplish this for a three-sphere run in which the no-slip boundary conditions are satisfied at four points on the surface of each sphere requires between 10 and 30 min of IBM 370/168 accounting time.

The numerical integration procedure used in this study is basically the same as that used by Leichtberg, Weinbaum, Pfeffer & Gluckman (1976). With the omission of the unsteady forces, the spheres may not be started from rest. Instead, the initial velocities are the quasi-steady velocities obtained from (2.12) and (2.13) for the initial configuration. The trajectory of each sphere in a vertical planar cluster of spheres is determined by integrating

$$d\tilde{\mathbf{s}}_j/d\tilde{t} = \tilde{\mathscr{V}}_j, \tag{5.1}$$

where $\tilde{\mathbf{s}}_j = \tilde{b}_j\,\hat{\mathbf{i}} + \tilde{d}_j\,\hat{\mathbf{k}}$ is the instantaneous distance of the centre of the jth sphere from the origin of a rectangular co-ordinate system which is at rest and $\tilde{\mathscr{V}}_j = \tilde{U}_j\,\hat{\mathbf{i}} + \tilde{W}_j\,\hat{\mathbf{k}}$ is the translational velocity of that sphere. Its angle of rotation α_j is obtained by integrating

$$d\alpha_j/d\tilde{t} = \tilde{\omega}_j, \tag{5.2}$$

where α_j is measured in radians and is positive in the counter-clockwise direction. The numerical integration is carried out as follows. If $\tilde{t}_0$ is an arbitrary time and $\Delta\tilde{t}$ is a

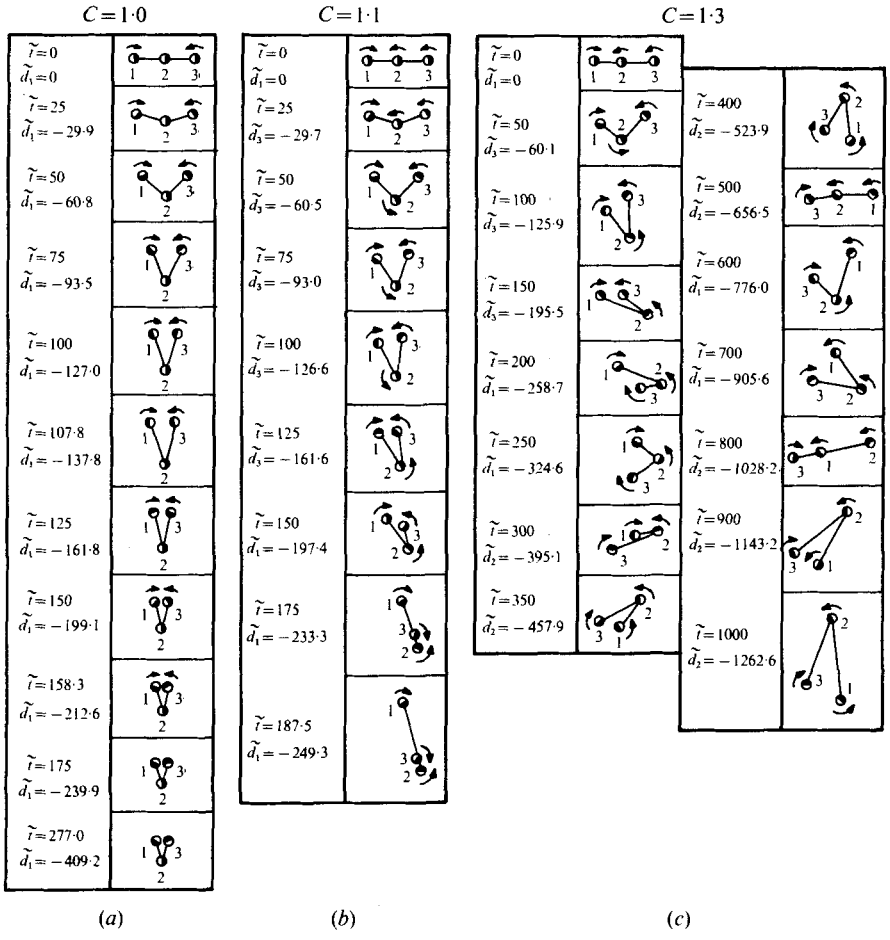

FIGURE 9. For legend see page 104.

finite but small time interval, the position and velocity of the jth sphere at time $\tilde{t}_0+\Delta\tilde{t}$ may be obtained in terms of the solution at $\tilde{t}_0$ by a Taylor expansion about $\tilde{t}_0$:

$$\tilde{\mathbf{s}}_j(\tilde{t}_0+\Delta\tilde{t}) = \tilde{\mathbf{s}}_j(\tilde{t}_0)+\dot{\tilde{\mathbf{s}}}_j(\tilde{t}_0)\,\Delta\tilde{t}+\tfrac{1}{2}\ddot{\tilde{\mathbf{s}}}_j(\tilde{t}_0)\,(\Delta\tilde{t})^2+\tfrac{1}{6}\dddot{\tilde{\mathbf{s}}}_j(\tilde{t}_0)\,(\Delta\tilde{t})^3+\ldots$$

$$= \tilde{\mathbf{s}}_j(\tilde{t}_0)+\tilde{\boldsymbol{\mathcal{V}}}_j(\tilde{t}_0)\,\Delta\tilde{t}+\tfrac{1}{2}\dot{\tilde{\boldsymbol{\mathcal{V}}}}_j(\tilde{t}_0)\,(\Delta\tilde{t})^2+\tfrac{1}{6}\ddot{\tilde{\boldsymbol{\mathcal{V}}}}_j(t_0)\,(\Delta\tilde{t})^3+\ldots, \tag{5.3}$$

$$\tilde{\boldsymbol{\mathcal{V}}}_j(\tilde{t}_0+\Delta\tilde{t}) = \tilde{\boldsymbol{\mathcal{V}}}_j(\tilde{t}_0)+\dot{\tilde{\boldsymbol{\mathcal{V}}}}_j(\tilde{t}_0)\,\Delta\tilde{t}+\tfrac{1}{2}\ddot{\tilde{\boldsymbol{\mathcal{V}}}}_j(t_0)\,(\Delta\tilde{t})^2+\tfrac{1}{6}\dddot{\tilde{\boldsymbol{\mathcal{V}}}}_j(\tilde{t}_0)\,(\Delta\tilde{t})^3+\ldots. \tag{5.4}$$

Solving (5.4) for $\dot{\tilde{\boldsymbol{\mathcal{V}}}}_j(\tilde{t}_0)$, substituting into (5.3) and neglecting terms of higher order than $(\Delta\tilde{t})^3$ yields

$$\tilde{\mathbf{s}}_j(\tilde{t}_0+\Delta\tilde{t}) = \tilde{\mathbf{s}}_j(\tilde{t}_0)+\tfrac{1}{2}[\tilde{\boldsymbol{\mathcal{V}}}_j(\tilde{t}_0)+\tilde{\boldsymbol{\mathcal{V}}}_j(\tilde{t}_0+\Delta\tilde{t})]\,\Delta\tilde{t}+\boldsymbol{\epsilon}_j(\tilde{t}_0), \tag{5.5}$$

where

$$\boldsymbol{\epsilon}_j(\tilde{t}_0) = -\tfrac{1}{12}\ddot{\tilde{\boldsymbol{\mathcal{V}}}}_j(t_0)\,(\Delta\tilde{t})^3 \tag{5.6}$$

is a correction used solely to estimate the error incurred by neglecting terms of order higher than $(\Delta\tilde{t})^2$. A similar equation may be obtained for the angle of rotation

$$\alpha_j(\tilde{t}_0+\Delta\tilde{t}) = \alpha_j(t_0)+\tfrac{1}{2}[\tilde{\omega}_j(\tilde{t}_0)+\tilde{\omega}_j(\tilde{t}_0+\Delta\tilde{t})]\,\Delta\tilde{t}+\epsilon_j(\tilde{t}_0), \tag{5.7}$$

where

$$\epsilon_j(\tilde{t}_0) = -\tfrac{1}{12}\ddot{\tilde{\omega}}_j(t_0)\,(\Delta\tilde{t})^3. \tag{5.8}$$

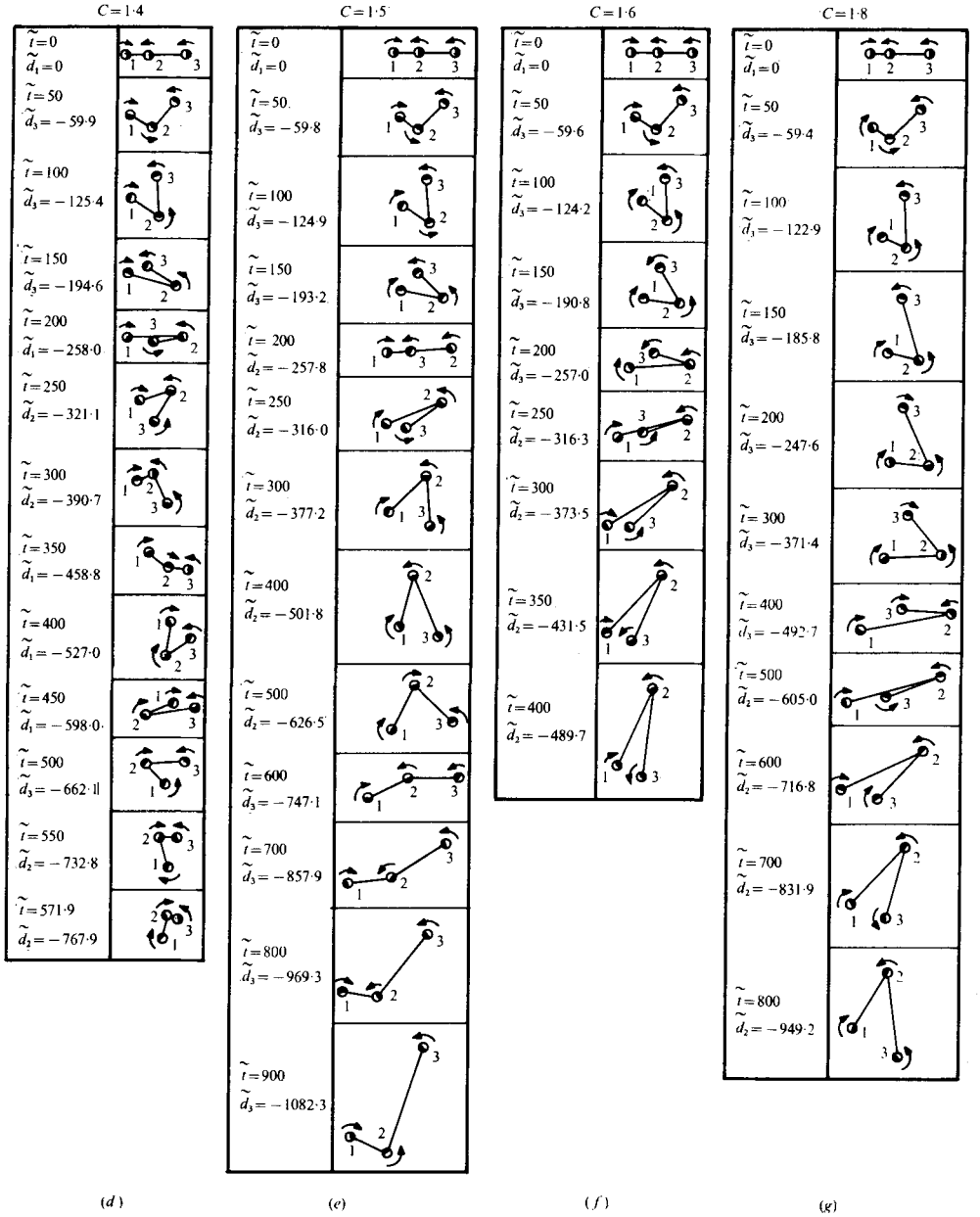

FIGURE 9. For legend see page 104.

The velocities $\tilde{\mathscr{V}}_j(\tilde{t}_0+\Delta\tilde{t})$ and $\tilde{\omega}_j(\tilde{t}_0+\Delta\tilde{t})$ are computed simultaneously by an iterative procedure which alternately solves for the positions and angles from (5.5) and (5.7) and for the translational and angular velocities from (2.12) and (2.13) using the collocation technique until convergence is achieved. Usually, only two iterations at each time step are required. Following convergence of the iteration procedure, the error for the

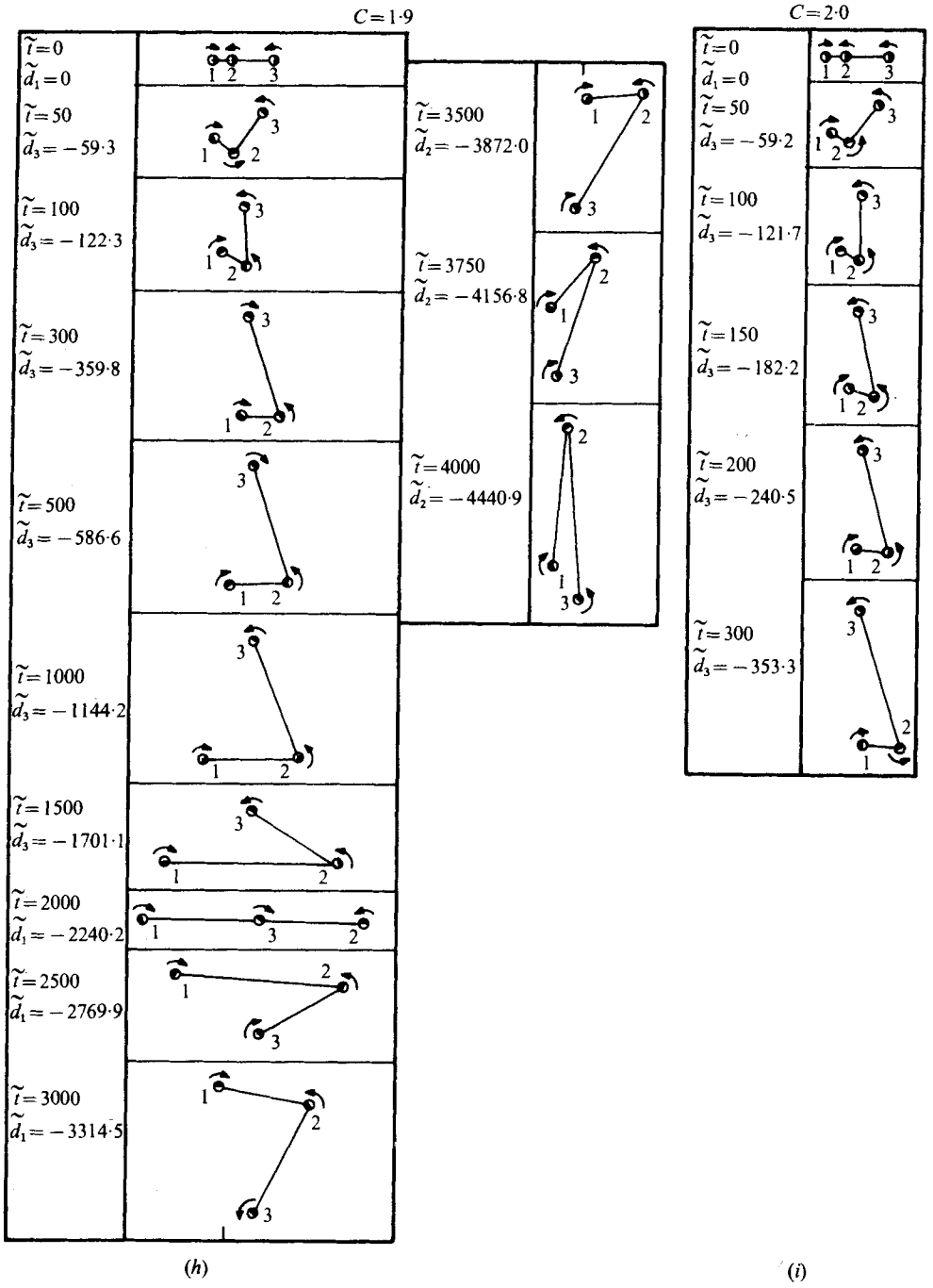

FIGURE 9. Horizontal chains of three unequally spaced spheres settling freely under gravity ($A+B$ = 6 diameters).

displacement and rotation is estimated from (5.6) and (5.8) written in finite-difference form. If any of these errors exceed preset error limits, the time interval is halved and the computations repeated. If, on the other hand, none of these errors exceeds 10 % of the preset error limits, the time interval $\Delta\tilde{t}$ is doubled before proceeding with the computations for the next time step. By doing this, computer time is kept to a minimum while the desired accuracy is maintained. All the numerical solutions to be presented in this section are based on the four-point collocation of (2.12) (figure 2*c*).

The simplest unsteady non-axisymmetric motion of a finite number of particles is that of three equal spheres settling freely in a vertical plane. Figure 9 shows a series of three-sphere numerical runs relative to a stationary reference frame in which the spheres begin from a horizontal-chain configuration. In all cases, the initial centre-to-centre distance between the two outer spheres is six diameters while the ratio

$$C \equiv \frac{\text{centre-to-centre distance from central to right outer sphere}}{\text{centre-to-centre distance from central to left outer sphere}} = \frac{B}{A} \tag{5.9}$$

is varied from 1·0 to 2·0 in increments of 0·1. These conditions were chosen since they correspond to the experimental studies of Jayaweera *et al.* (1964). Each figure is drawn to scale and the arrows indicate the instantaneous direction of the angular velocity of each sphere. The numbers to the left of each configuration indicate the total elapsed time $\tilde{t}$ and the distance $\tilde{d}_j$ fallen by the uppermost sphere measured in sphere radii.

Kynch (1959) discusses a special arrangement of three spheres in a vertical plane in which one sphere is midway between and above the other two, whose line of centres is horizontal. If the particles are equal, the two outer ones separate to allow the central sphere to pass between them and then close up behind it. Because of the reversibility of Stokes flow, the trajectory of the particles after they have formed a horizontal chain is a mirror image of the trajectory before. Thus it is necessary to consider only the motion of the spheres when they are released in a horizontal chain, i.e. $C = 1$ (figure 9*a*). As shown in figure 9 (*a*), the central sphere initially falls faster as the two outer spheres approach one another. A point is reached ($\tilde{t} = 107{\cdot}8$) where the three spheres fall with the same vertical speed; see figure 8. However, because of the non-vanishing horizontal drift, the outer spheres continue moving closer together. The outer spheres now form a doublet and begin falling faster than the central sphere. When the gap between the outer spheres reaches 0·1 diameter ($\tilde{t} = 158{\cdot}3$) the four-point collocation breaks down. However, qualitative results may be obtained beyond this point by artificially constraining the spheres from moving closer or rotating while allowing them to move apart and resume rotation when this is indicated. This extended solution shows that there is no tendency for the doublet formed by the outer spheres to separate, and the vertical distance between the doublet and the central sphere closes until a spacing is reached where all three spheres fall with equal velocity, creating a steady configuration. The run was discontinued after the ratio $\tilde{D}/\tilde{B}$ (see figure 8) was within 0·01 % of the critical value. It should be noted that the critical value of $\tilde{D}/\tilde{B}$ for $\tilde{B} = 1{\cdot}1$ shown in figure 9 (*a*) at $\tilde{t} = 277{\cdot}0$ is 3·567. This differs from the critical value of $\tilde{D}/\tilde{B} = 2{\cdot}715$ given by figure 8, since in the former case the two spheres forming the doublet have been artificially constrained from rotating or moving closer to each other.

A check on the overall accuracy of the numerical integration procedure may be

$C = B/A$	1·1	1·2	1·3	1·4	1·5	1·6	1·7	1·8	1·9	2·0	> 2·0
Hocking (1964) (theoretical)	1	1	—	—	2	—	—	—	—	1	3
Jayaweera *et al.* (1964) (experimental)	1	2	2	1	3	2	2	2	2	2	3
Present study	1	1	2†	1‡	3	2	2	†	2	3	3

† Inconclusive. ‡ $A + B = 10$ diameters.

TABLE 5. Sphere left behind for a horizontal chain of three unequally spaced spheres settling under gravity ($A + B = 6$ diameters).

made by running the three-sphere problem described in the previous paragraph in its entirety, i.e. beginning with $\tilde{B} = 1{\cdot}101$ for a horizontal doublet and placing a third sphere midway between and above the other two with $\tilde{D} = 4{\cdot}787$, which is the mirror image of the configuration shown in figure 9 (*a*) ($\tilde{t} = 158{\cdot}3$). Under these conditions the central sphere falls slower than the doublet. However, the leading pair spreads apart, allowing the central sphere to catch up such that the three spheres form a horizontal chain. If the run is carried out for a time period equal to twice the time required for the three spheres to form a horizontal chain, the final configuration should be a mirror image of the initial configuration. It was found that the total accumulated error for $\tilde{B}$ and $\tilde{D}$ at the end of the run was 0·08 % and 0·13 % of the initial values respectively, while the error in the angle of rotation of the outer spheres was $-0{\cdot}05$ %, of twice the value when the spheres formed a horizontal chain.

Hocking (1964) has presented qualitative results similar to those shown in figures 9 (*b–i*) using a single-reflexion weak-interaction theory in which the rotation of the spheres is neglected in an attempt to explain the qualitative experimental observations of Jayaweera *et al.* (1964) for several of the flow configurations shown in figure 9. In the experiments it was concluded that, for all values of C tested, one sphere in the cluster eventually remains behind the other two. These results as well as those of the present study are presented in table 5.† In general the agreement between the present theory and experiment is very good, especially considering the duration of some of the runs. Differences occur only for marginal values of C. The present study also shows that there are at least two narrow bands in the range of C, near $C = 1{\cdot}3$ and 1·8, for which the final configuration obtained from the numerical integration procedure indicates that the two leading spheres are very slowly spreading apart, which may eventually allow the trailing sphere to catch up after a long time period. These cases are labelled inconclusive in table 5. A run was made for $C = 1{\cdot}33$ and clearly showed that sphere 2 was left behind. The run for $C = 1{\cdot}4$ was discontinued after spheres 2 and 3 reached a gap of less than 0·1 diameter. The result shown for $C = 1{\cdot}4$ in table 5 is for $A + B = 10$ diameters.

While the qualitative agreement with experimental observation shown in table 5 is very encouraging, a quantitative comparison between the theoretical results and experimental measurements, especially of the small horizontal drift velocity, would be very reassuring owing to the uncertainty in the accuracy of the four-point colloca-

† Jayaweera *et al.* (1964) present their results in terms of ranges of values of C. It is not known whether their experiments were carried out for the specific values indicated in table 5.

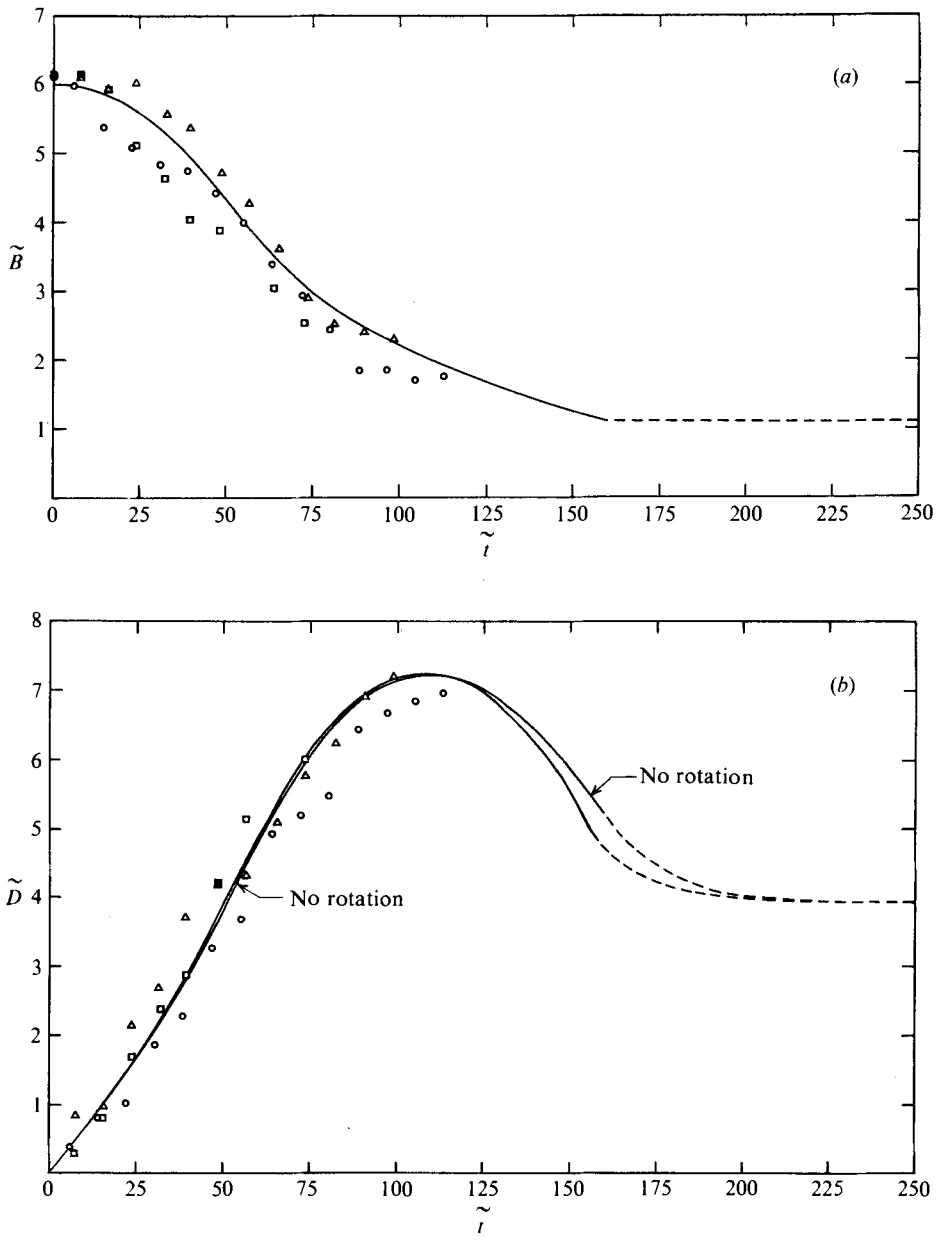

FIGURE 10. Comparison between theory and experiment for (*a*) the dimensionless horizontal sphere spacing $\tilde{B}$ and (*b*) the dimensionless vertical sphere spacing $\tilde{D}$. Experimental, $Re = 0{\cdot}011$: □, run 1; ○, run 2; △, run 3; ——, numerical solution; – – –, gap of doublet artificially constrained from becoming smaller than 0·1 sphere diameter in numerical solution.

tion solutions for this velocity component as discussed in relation to figure 4(*b*). Thus, as part of a larger experimental study of multiparticle Stokes flow interactions in our laboratory, Randall Wu and Zeev Dagan have conducted a series of careful measurements corresponding to the initial configuration depicted in figure 9(*a*). The experimental apparatus and the spheres used as well as the measurement technique are

described in Leichtberg, Weinbaum, Pfeffer & Gluckman (1976, pp. 600–601). Unfortunately, these commercially made nylon spheres had tiny internal bubbles with sufficient eccentricity to preclude accurate measurements of the small hydrodynamically generated angular velocities. After many trials three spheres with virtually identical quasi-steady settling velocities were obtained.

Figure 10 compares theory and experiment for the time-dependent variation of the relative horizontal and vertical spacings $\tilde{B}$ and $\tilde{D}$ as sketched in figure 8. Two sets of theoretical curves are shown, one in which the spheres are free to rotate and one in which the spheres are artificially constrained from rotating. The latter corresponds to the self-stabilizing configuration achieved in an internally eccentric sphere when the centre of gravity of the sphere lies below its centre of buoyancy. These two situations bracket the experimental conditions. The small differences in angular velocity involved are observed to have a small effect on the vertical spacing $\tilde{D}$, which grows with time, and an almost negligible effect on the horizontal spacing $\tilde{B}$. Optical distortion resulting from the curved walls of the settling tank introduces a measurement error of about 0·2 sphere diameters. The agreement between theory and experiment is good for both the horizontal and vertical spacing for the entire duration of the experimental runs. The time scale shown is the same as that used in figure 9, the measured runs corresponding to roughly the first 6 frames of figure 9(*a*). The length of the run, approximately 150 sphere diameters, was limited by the size of the apparatus and the spheres used. As noted in figure 10(*b*), there was a tendency for the vertical-spacing measurements to lag the theoretically predicted curves at the larger times in the experiments. This behaviour might be attributed to the omission of the Basset force in the numerical solution. In Leichtberg, Weinbaum, Pfeffer & Gluckman (1976) it is shown that these forces can cause discrepancies in vertical spacing which grow as $a\,Re\,\tilde{t}$ ($Re = 0{\cdot}011$ for the experiments shown) with increasing time. This effect would be much smaller for the horizontal drift because of the much smaller velocities and accelerations involved.

6. Some comments on the extension of the present technique to bounded flows

The multiple-sphere collocation technique described herein can be extended to a variety of bounded flow problems with both periodic and arbitrary particle spacing and planar symmetry using procedures very similar to those already developed in Wang & Skalak (1969) and Leichtberg, Pfeffer & Weinbaum (1976) respectively for axisymmetric flow. In either case one first transforms the boundary-value problem for the collocation technique to a form that is entirely equivalent to that already treated in the present study for planar multiple-sphere configurations. This procedure is briefly outlined below.

In place of (2.3), the fundamental equation for the velocity field for a system of N spheres lying in a plane of symmetry, with an arbitrary symmetric upstream flow and planar or cylindrical boundaries, is given by the linear superposition

$$\mathbf{V} = \mathbf{V}_\infty + \sum_{j=1}^{M} \mathbf{V}_{wj} + \sum_{j=1}^{N} \sum_{n=1}^{\infty} \Big[\nabla \times (\mathbf{r}_j \chi_{-(n+1)}) + \nabla \Phi_{-(n+1)} - \frac{(n-2)}{2\mu n(2n-1)} r_j^2 \nabla P_{-(n+1)} + \frac{(n+1)}{\mu n(2n-1)} \mathbf{r}_j P_{-(n+1)} \Big], \quad (6.1)$$

where in view of the planar symmetry [see (2.4) and (2.5)]

$$\begin{Bmatrix} \chi_{-(n+1)} \\ \phi_{-(n+1)} \\ P_{-(n+1)} \end{Bmatrix} = \sum_{m=0}^{n} P_n^m(\zeta_j) \frac{1}{r_j^{n+1}} \left[\begin{Bmatrix} 0 \\ C_{jmn} \\ E_{jmn} \end{Bmatrix} \cos m\phi_j + \begin{Bmatrix} B_{jmn} \\ 0 \\ 0 \end{Bmatrix} \sin m\phi_j \right]. \tag{6.2}$$

Here $\mathbf{V}_\infty$ is the specified flow at upstream infinity and $\mathbf{V}_{wj}$ the velocity disturbance due to each confining boundary. The latter is a Fourier series or integral of the fundamental separable solutions of the Stokes-flow equation written in rectangular or cylindrical co-ordinates depending on the shape of the boundary and the particle geometry.

For an infinite periodic array of spheres with arbitrary spacing aligned at any normal distance from, but parallel to, the confining walls the expression for $\mathbf{V}_{wj}$ is an infinite series containing three sets of unknown coefficients F_{nj}, G_{nj} and H_{nj}. The harmonic functions (6.2) representing the velocity disturbance due to each sphere are now written in the co-ordinate system corresponding to the boundary chosen and the total velocity $\mathbf{V}$ set equal to zero to satisfy the no-slip boundary conditions along the entire co-ordinate surface of each confining boundary present. These no-slip conditions provide three equations, one for each velocity component, which are to be satisfied at every point along the confining boundary. This is accomplished by multiplying each of the three boundary equations by the infinite set of appropriate orthogonal functions and integrating over the interval of periodicity. This procedure leads to an infinite ordered system of three linear algebraic equations in which sets of F_{nj}, G_{nj} and H_{nj} are related to linear matrices involving sums of the unknown sphere coefficients C_{jmn}, E_{jmn} and B_{jmn}. The solutions for the F_{nj}, G_{nj} and H_{nj} are now substituted back into the expressions for the $\mathbf{V}_{wj}$ in (6.1) and the no-slip boundary conditions satisfied at discrete points on the surface of each sphere as described in § 2. The resulting set of equations is entirely equivalent to the linear matrix equation (2.12) for the unknown sphere coefficients C_{jnm}, E_{jnm} and B_{jmn} obtained in the present study.

The treatment of a confined system of spheres in an arbitrary planar configuration of spheres is similar in concept to that just outlined for periodic flow geometries, but mathematically more involved. The velocity disturbance $\mathbf{V}_{wj}$ describing each confining boundary is a Fourier integral involving a continuous distribution of unknown Fourier coefficients $F_j(t)$, $G_j(t)$ and $H_j(t)$, where t is the transform variable. The procedure for determining these coefficients in terms of the unknown sphere coefficients C_{jmn}, E_{jmn} and B_{jmn} by employing the no-slip boundary conditions along the surface of each confining boundary is the same as that just described for periodic confined flows except that one has to evaluate the Fourier integral transform of the wall disturbance. While it is possible to perform these integrations analytically for simple co-ordinate geometries and thus find closed-form solutions for $F_j(t)$, $G_j(t)$ and $H_j(t)$ the evaluation of the inversion integrals is very laborious and must be performed numerically. The same difficulty arises for axisymmetric flow and is described in detail in Leichtberg, Pfeffer & Weinbaum (1976). Thus, if one wishes to study the arbitrary off-axis motion of a single sphere in a circular cylinder, past experience has shown that it is considerably simpler to approximate this problem as a periodic array of identical spheres in which the intersphere spacing is large (say 20 sphere diameters) than to use an infinite-boundary Fourier-integral approach. This simplification obviously does not apply to finite clusters of two or more spheres. All the preceding comments apply equally well if

the particles are spheroids instead of spheres except that (6.2) is replaced by spheroidal harmonic functions (Jeffery 1922). One interesting biological problem in this regard is the tumbling of a red cell near a planar boundary.

The collocation technique used to solve the matrix equation which replaces (2.12) for bounded systems is virtually identical to that described herein for unconfined spheres. In essence, the undetermined coefficients in the series solution for each sphere are used to reduce to zero, on the surface of the sphere, the velocity disturbance produced by the incident stream, and all other boundaries, whether they originate from another sphere or a confining wall. Thus the general guidelines for the selection of boundary points are not altered. The arbitrary planar motion of a single confined sphere or periodic array of spheres relative to infinite straight boundaries can be separated into motions parallel and perpendicular to the confining wall. Thus, for these cases the highly accurate truncation techniques described for the purely horizontal or vertical motion of two spheres in §3 can be expected to apply equally well. On the other hand, for the planar asymmetric motion of finite arrays of two or more spheres one would expect to find equivalent truncation difficulties to those described herein for the settling of two or more spheres at an arbitrary orientation.

In closing, the authors wish to mention two confined problems they are currently investigating. One is the motion of a sphere of arbitrary size between planar parallel walls. This problem has the important application of the diffusion of solute molecules along the intercellular channels between adjacent cells that have been observed in electron microscopic studies of endothelial membranes. The second problem is the motion of a sphere at the entrance to a circular hole in a planar wall. The application here is to the molecular sieving effects that have been observed in both artificial and biological membranes.

The authors wish to thank the National Science Foundation for supporting this research under grant no. GK-40802. P. Ganatos wishes to thank Dr Michael S. Kolansky for his help in the use of the IBM 370/168 computer system and The City University of New York Computer Center for the use of their facilities. The above work has been performed in partial fulfilment of the requirements for the Ph.D. degree of P. Ganatos from The School of Engineering of The City College of The City University of New York.

REFERENCES

CHEN, T. C. & SKALAK, R. 1970 *Appl. Sci. Res.* **22**, 403.

DAVIS, A. M. J., O'NEILL, M. E., DORREPAAL, J. M. & RANGER, K. B. 1976 *J. Fluid Mech.* **77**, 625.

GANATOS, P. 1977 Ph.D. dissertation, City University of New York.

GLUCKMAN, M. J., PFEFFER, R. & WEINBAUM, S. 1971 *J. Fluid Mech.* **50**, 705.

GLUCKMAN, M. J., WEINBAUM, S. & PFEFFER, R. 1972 *J. Fluid Mech.* **55**, 677.

GOLDMAN, A. J., COX, R. G. & BRENNER, H. 1966 *Chem. Engng Sci.* **21**, 1151.

HAPPEL, J. & BRENNER, H. 1973 *Low Reynolds Number Hydrodynamics*, 2nd ed. Noordhoff.

HOCKING, L. M. 1964 *J. Fluid Mech.* **20**, 129.

HYMAN, W. A. & SKALAK, R. 1972 *Appl. Sci. Res.* **26**, 27.

JAYAWEERA, K. O. L. F., MASON, B. J. & SLACK, H. W. 1964 *J. Fluid Mech.* **20**, 121.

JEFFERY, G. B. 1922 *Proc. Roy. Soc.* A **102**, 161.

KYNCH, G. J. 1959 *J. Fluid Mech.* **5**, 193.

LAMB, H. 1945 *Hydrodynamics*, 6th edn. Dover.

LEICHTBERG, S., PFEFFER, R. & WEINBAUM, S. 1976 *Int. J. Multiphase Flow* **3**, 147.

LEICHTBERG, S., WEINBAUM, S. & PFEFFER, R. 1976 *Biorheol.* **13**, 165.

LEICHTBERG, S., WEINBAUM, S., PFEFFER, R. & GLUCKMAN, M. J. 1976 *Phil. Trans. Roy. Soc.* A **282**, 585.

O'BRIEN,, V. 1968 *A.I.Ch.E. J.* **14**, 870.

SKALAK, R., CHEN, P. H. & CHIEN, S. 1972 *Biorheol.* **9**, 67.

STIMSON, M. & JEFFERY, G. B. 1926 *Proc. Roy. Soc.* A **111**, 110.

WANG, H. & SKALAK, R. 1969 *J. Fluid Mech.* **38**, 75.

YOUNGREN, G. K. & ACRIVOS, A. 1975 *J. Fluid Mech.* **69**, 377.